MIT Open Access Articles

The impact of feedback on cosmological gas accretion

Massachusetts Institute of Technology

The impact of feedback on cosmological gas accretion

Dylan Nelson[1]⋆, Shy Genel[1], Mark Vogelsberger[2], Volker Springel[3,4],
Debora Sijacki[5], Paul Torrey[2,6], Lars Hernquist[1]

[1]*Harvard-Smithsonian Center for Astrophysics, 60 Garden Street, Cambridge, MA, 02138, USA*
[2]*Kavli Institute for Astrophysics and Space Research, Department of Physics, MIT, Cambridge, MA 02139, USA*
[3]*Heidelberg Institute for Theoretical Studies, Schloss-Wolfsbrunnenweg 35, 69118 Heidelberg, Germany*
[4]*Zentrum für Astronomie der Universität Heidelberg, ARI, Mönchhofstr. 12-14, 69120 Heidelberg, Germany*
[5]*Institute of Astronomy and Kavli Institute for Cosmology, University of Cambridge, Madingley Road, Cambridge CB3 0HA, UK*
[6]*TAPIR, Mailcode 350-17, California Institute of Technology, Pasadena, CA 91125, USA*

6 March 2015

ABSTRACT

We investigate how the way galaxies acquire their gas across cosmic time in cosmological hydrodynamic simulations is modified by a comprehensive physical model for baryonic feedback processes. To do so, we compare two simulations – with and without feedback – both evolved with the moving mesh code AREPO. The feedback runs implement the full physics model of the Illustris simulation project, including star formation driven galactic winds and energetic feedback from supermassive blackholes. We explore: (a) the accretion rate of material contributing to the net growth of galaxies and originating directly from the intergalactic medium, finding that feedback strongly suppresses the raw, as well as the net, inflow of this "smooth mode" gas at all redshifts, regardless of the temperature history of newly acquired gas. (b) At the virial radius the temperature and radial flux of inflowing gas is largely unaffected at $z = 2$. However, the spherical covering fraction of inflowing gas at $0.25\,r_{\rm vir}$ decreases substantially, from more than 80% to less than 50%, while the rates of both inflow and outflow increase, indicative of recycling across this boundary. (c) The fractional contribution of smooth accretion to the total accretion rate is lower in the simulation with feedback, by roughly a factor of two across all redshifts. Moreover, the smooth component of gas with a cold temperature history, is entirely suppressed in the feedback run at $z < 1$. (d) The amount of time taken by gas to cross from the virial radius to the galaxy – the "halo transit time" – increases in the presence of feedback by a factor of $\simeq 2\text{-}3$, and is notably independent of halo mass. We discuss the possible implications of this invariance for theoretical models of hot halo gas cooling.

Key words: cosmology: theory – galaxies: evolution, formation, haloes – methods: numerical

1 INTRODUCTION

Over the past decade, numerical simulations modelling the evolution of gas in a ΛCDM cosmology have made it clear that the process by which galaxies acquire their baryons across cosmic time evades a satisfactory understanding. In the "classical" theory of collapse and virialisation, gas from the intergalactic medium shock-heats to the virial temperature of a dark matter halo, subsequently forming a hot, pressure supported atmosphere in approximate equilibrium (Rees & Ostriker 1977; Silk 1977; White & Rees 1978). The

timescale of energy loss from radiative cooling determines the rate at which gas can cool into the halo centre (White & Frenk 1991), and indeed whether or not a stable virial shock can exist at all (Birnboim & Dekel 2003).

Numerical simulations over the past decade (starting with Katz et al. 2003; Abadi et al. 2003; Kereš et al. 2005) have shown that gas accretion in the cosmological context, without the luxury of spherical symmetry, is significantly more complex. They found that (i) coherent streams of gas can provide strong fuelling for star formation over relatively small solid angles of the virial sphere, and (ii) such streams could potentially remain cold and avoid heating up to the virial temperature, even for haloes massive enough

⋆ E-mail: dnelson@cfa.harvard.edu

to support a quasi-static hot atmosphere. Such flows are a natural consequence of the "cosmic web" of large scale structure, particularly at high redshift ($z > 2$), and provide an intriguing avenue for gas accretion distinct from classic hot halo cooling. Aspherical gas inflow has been connected to many key questions in galaxy formation, including the growth of the stellar populations of galaxies (e.g. Oppenheimer et al. 2010), their morphological transformations (Sales et al. 2012; Cen 2014), kinematics (Genel et al. 2012), and star formation properties (Gabor & Bournaud 2014; Sánchez Almeida et al. 2014). It has also been looked at in terms of the acquisition of angular momentum (Danovich et al. 2012; Stewart et al. 2013; Danovich et al. 2014), including the connection to preferred directions imposed by the filaments of large scale structure (Dubois et al. 2014), and the feeding of supermassive blackhole accretion (Dubois et al. 2012b; Bellovary et al. 2013; Feng et al. 2014).

Smoothed particle hydrodynamics (SPH) simulations were the first to address the question of gas accretion modes in a cosmological context. Leveraging the quasi-Lagrangian nature of the numerical scheme, they could use the past temperature history of each gas element to differentiate between hot and cold mode accretion. It was found that the maximum past temperature of smoothly accreted gas is bimodal, the dominant contribution arising from gas which has never experienced significant heating during infall to the galaxy (Kereš et al. 2005).

However, caution is warranted. In our previous study (Nelson et al. 2013) we compared the outcome of "classic" SPH simulations and those run with the newer moving mesh code AREPO. At $z = 2$ we found a decrease in the accretion rate of cold gas, by a factor of ~ 2 at $M_{\rm halo} \simeq 10^{11}\,{\rm M}_\odot$. We also found, at this same mass, an order of magnitude larger accretion rate of gas with significant past heating. These discrepancies grew even more significant for more massive haloes. We attributed the drop in the cold accretion rate to a large population of numerical "blobs" (Torrey et al. 2012) which efficiently deliver cold gas to central galaxies in the SPH simulations, but are completely absent in the moving mesh calculations. The increase in the hot accretion rate was dominated by more efficient cooling from halo gas in AREPO, where spurious heating from the dissipation of turbulent energy on large scales prevents the correct behaviour in SPH (Bauer & Springel 2012). Filamentary flows in the AREPO haloes were found to be warmer and more diffuse, and did not generally persist as strongly to small radii.

Grid-based adaptive mesh refinement (AMR) simulations have also been interpreted as being in agreement with respect to the importance of a filamentary, cold accretion mode in massive systems at high redshift (Ocvirk et al. 2008; Dekel et al. 2009; Agertz et al. 2009), albeit with two potentially important limitations. In particular, these studies have often not used any form of Lagrangian tracer to follow the thermal and dynamical history of accreting gas, which would permit a more direct comparison with particle hydrodynamics codes. With the notable exception of Ocvirk et al. (2008), they have also generally focused on targeted, "zoom" simulations of individual haloes, where the significant halo-to-halo variation between codes (e.g. Vogelsberger et al. 2012) can make broadly applicable conclusions difficult. Regardless of hydrodynamical method, robust conclu-

sions are difficult to draw from a single simulated halo, or a small sample of such haloes.

These findings made it clear that numerical deficiencies in the standard formulation of SPH used in past studies significantly biased previous quantitative conclusions as to the relative importance of cold streams or cold mode accretion (also problematic are issues with formal numerical convergence, as discussed in Zhu et al. 2014). However, in this previous comparison work we included only a simple model for baryonic physics, appropriate to make an even-handed comparison to past work, but lacking the physical fidelity of modern cosmological simulations. The large question left outstanding was then: what impact, if any, does feedback associated with galaxy formation have on the process of gas accretion. Current state-of-the-art cosmological simulations have reached the point where they can evolve a significant volume of the universe down to $z = 0$, while simultaneously resolving the structure of individual galaxies, and reproducing a broad range of observational constraints (Khandai et al. 2014; Vogelsberger et al. 2014b; Schaye et al. 2014). One of the many investigations related to galaxy formation and evolution that they enable is a study of baryonic accretion.

At the outset, it would seem entirely plausible that the accretion rates and the inflow of gas from the intergalactic medium would be quite sensitive to feedback processes. The impact could be either direct or indirect, or both. For instance, inflowing streams could be disrupted by spatially coincident outflows, such that the net mass flux entirely reversed direction. Or, energy injection from feedback could heat up the the surrounding hot halo gas, leading to a modification of the thermal history of inflow due to mixing. Alternatively, it would also seem plausible that feedback could have relatively little effect. For instance, star formation driven winds with non-isotropic outflow may simply evolve to occupy different regions of the virial volume than inflowing streams.

Recently, simulations have begun to investigate the additional complexity when feedback and galactic scale outflows are included (beginning with Oppenheimer et al. 2010; Faucher-Giguère et al. 2011; van de Voort et al. 2011a). Conclusions as to their impact have been somewhat mixed, which undoubtedly arise from a combination of different feedback implementations, numerical methods, contexts, and interpretations. In brief review, Brooks et al. (2009) simulated five haloes, included a delayed cooling, supernova blastwave feedback model, but did not explicitly consider the impact of the feedback in GASOLINE, and in general found results consistent with Kereš et al. (2005). Oppenheimer et al. (2010) included a kinetic galactic wind model in cosmological SPH simulations and concluded that recycled gas accretion is in fact the dominant accretion mechanism at $z \lesssim 1$, with minimal effect on high redshift accretion. Faucher-Giguère et al. (2011) included a constant velocity galactic wind model, finding that net accretion rates measured as instantaneous mass fluxes could be substantially affected. van de Voort et al. (2011a) found that while the gas accretion rates onto haloes was relatively robust against the presence of feedback, the rates onto galaxies themselves depended sensitively on stellar winds as well as metal-line cooling. van de Voort et al. (2011b) studied the impact of AGN feedback on inflow and found that it preferentially pre-

vented hot mode gas, with high maximum past temperature, from cooling from the halo onto the galaxy. Stewart et al. (2011) simulates two relatively massive haloes, including the supernova blastwave feedback model, but notes this has little impact at the simulated mass scale, and does not consider how it modifies gas accretion nor AGN effects. Dubois et al. (2012a) investigated AGN feedback at high redshift in one halo, and found that large-scale hot superwinds could morphologically disturb cold filaments and quench cold diffuse accretion. Murante et al. (2012) used a thermal supernova feedback scheme, and found that additional heating of cold inflow due to this feedback gave rise to a significant accretion rate of intermediate temperature gas. Most recently, Woods et al. (2014) includes a combined delayed cooling supernova and early stellar feedback model, finding that overall gas accretion rates did not change with strong feedback, while the balance between cold and hot components did. Finally, Übler et al. (2014) implements a hybrid thermal/kinetic stellar feedback scheme and finds strong outflows generate substantially higher raw accretion rates, and that recycled material dominates galactic gas accretion at $z < 1$.

As a caveat, we note that the same numerical issues explored in the "moving mesh cosmology" series (Vogelsberger et al. 2012; Sijacki et al. 2012; Kereš et al. 2012; Nelson et al. 2013) that compromised the accuracy of SPH studies of gas inflow will also affect the interaction of outflowing ejecta and wind material with both halo and filamentary gas. Further, because hot gas in our AREPO simulations cools more efficiently than in classical SPH, the energy input from feedback required to prevent over-cooling is even larger than in previous simulations, implying that the impact on gas accretion could be significantly altered. We are therefore motivated to extend previous investigations with the current study, which combines a comprehensive, validated feedback model with an accurate and robust numerical technique in a systematic comparison.

This paper contrasts two simulations, realisations of the same initial conditions evolved with the moving mesh code AREPO. We compare populations of haloes and galaxies across cosmic time, contrasting the state and history of accreting gas between two runs, with and without feedback. In Section 2 we describe the simulation technique and analysis methodology. Section 3 addresses the rate and history of primordial gas accretion, while Section 4 compares the instantaneous state of gas in haloes. Section 5 considers the timescale of accretion through the halo. Finally, Sections 6 and 7 discuss our results and their implications, and summarise our conclusions.

2 METHODS

2.1 The Simulations

In this work we compare two simulations, "with" and "without" feedback, which have several common features. Both employ the AREPO code (Springel 2010) to solve the problem of ideal continuum hydrodynamics coupled with self-gravity. An unstructured, Voronoi tessellation of the simulation domain provides a spatial discretization for Godunov's method with a directionally un-split MUSCL-Hancock scheme (van Leer 1977) and an exact Riemann

solver, yielding second order accuracy in space. Since the mesh generating sites can be allowed to move, herein with a velocity tied to the local fluid velocity modulo mesh-regularization corrections, this numerical approach falls under the Arbitrary Lagrangian-Eulerian (ALE) class. Gravitational forces are handled with the split Tree-PM approach, whereby long-range forces are calculated with a Fourier particle-mesh method, medium-range forces with a hierarchical tree algorithm (Barnes & Hut 1986), and short-range forces with direct summation. A local, predictor-corrector type, hierarchical time stepping method yields second order accuracy in time. Numerical parameters secondary to our current investigation – for example, related to mesh regularization or gravitational force accuracy – are detailed in Springel (2010) and Vogelsberger et al. (2012), and are unchanged between the two simulation sets.

Both simulations evolve the same initial condition, a random realisation of a WMAP-7 consistent cosmology ($\Omega_{\Lambda,0} = 0.73$, $\Omega_{m,0} = 0.27$, $\Omega_{b,0} = 0.045$, $\sigma_8 = 0.8$ and $h = 0.7$) in a periodic cube of side-length $20h^{-1}$ Mpc $\simeq 28.6$ Mpc, from a starting redshift of $z = 99$ down to $z = 0$. Each includes 512^3 dark matter particles, an equal number of initial gas cells, and a minimum of 5×512^3 tracers (discussed below). The mean baryon mass is $1.1 \times 10^6 \, \mathrm{M_\odot}$, and the dark matter particle mass is $5.3 \times 10^6 \, \mathrm{M_\odot}$. The Plummer equivalent comoving gravitational softening lengths for dark matter and stars are 1.4 kpc, and gas cells have adaptive softening lengths equal to 2.5 times their volume-equivalent spherical radius. A redshift-dependent, spatially uniform, ionizing UV background field (Faucher-Giguère et al. 2009) is included as a heating source. Star formation and the associated ISM pressurisation from unresolved supernovae are included with an effective equation of state modelling the ISM as a two-phase medium, following Springel & Hernquist (2003). Gas elements are stochastically converted into star particles when the local gas density exceeds a threshold value of $n_H = 0.13 \, \mathrm{cm^{-3}}$. All of the simulations considered in this work disregard the possible effects of radiative transfer, magnetic fields, and cosmic rays.

The **no feedback runs** ("noFB") with "simple physics" additionally account for optically thin radiative cooling assuming a primordial H/He ratio (Katz et al. 1996). They do not include metal line cooling, any resolved stellar feedback that would drive galactic-scale wind, nor any treatment of black holes or their associated feedback. This is the same simulation presented in Nelson et al. (2013), where it was used in comparison to GADGET (SPH) results.

The **feedback runs** ("FB") implement, unchanged, the fiducial physical model and associated parameter values of the Illustris simulation (Vogelsberger et al. 2014b,a; Genel et al. 2014) applied to the same initial conditions as our previous work, allowing object by object comparison. Complete details of the physics included in the model, as well as its tuning and validation, are described in Vogelsberger et al. (2013) and Torrey et al. (2014). We describe here in some detail those aspects of the model which most strongly influence gas accretion.

First, we include the radiative cooling contribution from metal lines, where heavy elements are produced from supernovae Ia/II and AGB stars in stellar population evolution modelling (Thielemann et al. 1986; Portinari et al. 1998; Karakas 2010). In the absence of additional heat-

ing sources, this can increase the cooling rate $\Lambda(n, T, Z, \Gamma)$, for solar metallicity by an order of magnitude between $10^{4.5} \, \mathrm{K} < T_{\mathrm{gas}} < 10^{6.5} \, \mathrm{K}$, mainly due to the contribution of O, Ne and Fe (Sutherland & Dopita 1993; Wiersma et al. 2009), enhancing cooling from the hot halo and the buildup of stellar mass.

To balance efficient cooling in the simulations, further exacerbated by metals, we include energetic feedback from star formation driven winds as well as supermassive black holes – dominant in haloes less and more massive than $M_\star$, respectively. Stellar winds are generated directly from star-forming gas, with velocity $v_w = 3.7\sigma_{\mathrm{dm}}$ where σ_{dm} is the local 1D dark matter velocity dispersion, which scales with the circular velocity maxima and so host (sub)halo total mass. In practice, gas cells are probabilistically converted into a wind-phase gas cell/particle, which interacts gravitationally but not hydrodynamically, until it reaches either a density threshold or a maximum travel time. Specifically, 0.05 times the star formation threshold in density, or 0.025 times the current Hubble time. This typically occurs just outside the disk – that is, deep within the halo. At this point, the mass, momentum, metals, and internal energy are deposited into the gas cell in which the wind particle is located.

The energy-driven wind has a mass loading factor $\eta_w \propto v_w^{-2}$ (thereby decreasing with halo mass) and is assigned a "bipolar" outflow direction, given by the cross product of its original velocity and the gradient of the local potential. Since the wind speed is in general slightly less than the escape speed, this implementation can generate a strong "galactic fountain" effect of recycled material returning to the galaxy (Oppenheimer et al. 2010; Davé et al. 2012). As a result, it can also strongly modify the temperature and velocity structure of gas in the inner halo.

The second form of feedback originates in supermassive black holes (SMBHs, following Sijacki et al. 2007), which are seeded with a mass of $1.4 \times 10^5 \, \mathrm{M}_\odot$ in massive haloes above $7 \times 10^{10} \, \mathrm{M}_\odot$ and are effectively sink particles which grow through gas accretion and merging. When accretion onto the black hole is below 0.05 of the Eddington rate, a radio-mode model injects highly bursty thermal energy equal to 0.07 of the accreted rest mass energy in large ($\simeq 50$ kpc) bubbles. When the accretion rate is above this fraction, a quasar-mode model injects thermal energy into nearby gas cells, with a lower coupling efficiency of 0.01 and a smoother time profile. For accretion rates approaching Eddington, a third, radiative form of feedback modifies the cooling rate for gas in the vicinity of the BH, assuming an optically-thin $1/r^2$ attenuation. In the halo mass regime where BH feedback becomes important, the radio-mode channel generates high velocity, high temperature outflows which influence gas at larger radii than the stellar feedback driven winds – out to the virial radius and into the intergalactic medium.

There are three other minor changes with respect to the noFB configuration, required to match the fiducial Illustris model. First, we modify the equation of state parameter (Springel & Hernquist 2003) from $q = 1$ to $q = 0.3$, which interpolates between the effective EOS and an isothermal EOS of 10^4 K with weights of 0.3 and 0.7, respectively, in order to avoid over pressurising the ISM of star-forming gas. Secondly, we decouple the comoving gravitational softening lengths of the gas and stars from that of the dark matter at $z = 1$, allowing the former to decrease by a further factor of two down to $z = 0$. Finally, we include a correction for self-shielding of dense gas from the UV background (Rahmati et al. 2013).

2.2   Monte Carlo Tracers

Both simulations include our new "Monte Carlo tracer particle" technique (Genel et al. 2013) in order to follow the evolving properties of gas elements over time. This is a probabilistic method, where tracers act as unique tags in association with parent cells or particles. They have no phase space coordinates, but are instead exchanged between parents based explicitly on the corresponding mass fluxes. By locating a subset of their unique IDs at each snapshot we can, by reference to the gas cells in which the tracers reside (their parents), reconstruct their spatial trajectory or thermodynamic history. Furthermore, at each computational timestep every active tracer updates a record of its maximum temperature, density, Mach number and entropy, as well as the time of these events, enabling us to investigate these values with timestep-level resolution.

We extend the Monte Carlo tracer approach to include mass transfer between all baryonic components present in the simulations in a fully self-consistent manner. That is, tracers can reside in gas cells, star particles, wind-phase cells, and black holes, and exchange between these components in exactly the same ways that baryonic mass is exchanged during the simulation. In particular:

(i) Gas cell to gas cell transfer via finite volume fluxes, refinement and derefinement.

(ii) Gas cell to star particle via star formation, and the reverse during stellar mass return.

(iii) Gas cell to/from wind-phase during the generation/recoupling of star formation driven galactic winds.

(iv) Gas cell to black hole as a result of BH accretion, and between two black holes during a merger.

This allows us to follow the flow of mass through all baryonic phases which are present. Finally, to explore the role of stellar feedback driven winds and recycling, each tracer also records the last time of exchange to a star/wind particle from gas, and the reverse, as well as a counter of the number of times it has been incorporated into a wind.

2.3   Post-processing

We identify dark matter haloes and their gravitationally bound substructures using the SUBFIND algorithm (Springel et al. 2001; Dolag et al. 2009) which is applied on top of a friends-of-friends cluster identification. We refer to the most massive substructure in each FoF group as the halo itself, and consider accretion onto such haloes and the central galaxies hosted therein. We follow the evolving positions and properties of haloes over time by constructing a basic merger tree as in Nelson et al. (2013), where only the "main progenitor branch" (MPB) is needed. For each halo, we restrict our analysis of accretion to the time period over which this main branch is robustly determined.

For each of a finite number of analysis redshifts, spanning $z = 0$ to $z = 5$, we perform a set of independent, identical analysis tasks. For all tracers (of all parent types) in

all haloes at that redshift, we walk backwards and record the most recent time and direction of several particular radial crossings. We take $r_{vir} = r_{200,crit}$ the radius enclosing a mean overdensity 200 times the critical density. We label the inward crossing times of two important radii, $0.15\,r_{vir}$ (representative of the outer boundary of the galaxy), and $1.0\,r_{vir}$ (representative of the outer boundary of the halo) the "most recent incorporation time" into the galaxy and the "most recent accretion time" into the halo, respectively. For these same two radii, we also record the earliest – that is, highest redshift – such crossing. We label the $0.15\,r_{vir}$ crossing as the "first incorporation time", and the $1.0\,r_{vir}$ crossing as the "first accretion time". We discuss the calculation of accretion rates based on these quantities in the following section.

Each tracer also records the virial temperature of its parent halo at the time of first accretion, labelled $T_{vir,acc}$. We compare this value against T_{max}, the maximum temperature of a tracer between the start of the simulation and the time of its first incorporation. This corresponds to the time at which each tracer accretes into the direct main progenitor of the central galaxy of the halo. As a result, the procedure is sensitive to virial shock heating in the MPB, as well as virial shock and feedback related heating in satellites prior to first incorporation, but not heating due to wind recycling after incorporation into the central galaxy.

In addition, we also separate all accreted tracers into one of three disjoint "modes" of accretion: smooth, clumpy, or stripped, according to the following definitions applied at the time of first accretion. Smooth: not a member of any resolved substructure, other than a MPB halo, and likewise at all previous times. Clumpy: gravitationally bound to any resolved substructure which is not a MPB halo. Stripped: otherwise smooth, but gravitationally bound to some resolved substructure other than the MBP at any previous time. In addition to these three modes, each tracer is also flagged as being "recycled" if it has ever been part of a stellar feedback driven wind at some previous time.

We note that identification of the "clumpy" component – that is, the merger contribution – includes only *resolved* substructure. The combination of simulation resolution and group finder implies a minimum halo mass which can be identified. For the conclusions presented herein, this is $M_{halo} \geqslant 10^{7.8}\,M_\odot$, meaning that for the halo mass range we consider all mergers with mass ratio above $\simeq 10^{-3}$ are correctly identified as a clumpy mode. The contribution of unresolved mergers below this level is expected to be negligible (see Kereš et al. 2005; Genel et al. 2009), and we have further verified that the associated conclusions are qualitatively unchanged in an identical simulation with a factor of eight lower mass resolution.

3 RATE AND MODE OF GAS ACCRETION

In this section we compare the rate and mode of cosmological gas infall across cosmic time between the two simulations, with and without our fiducial feedback model. The presence of star formation driven galactic winds and AGN feedback, particularly in the radio-mode, generates significant radial velocity in the baryonic component of haloes. Outflows with high outward bulk motion in turn trigger "galactic foun-

tain" behaviour, with significant gas mass returning after some time delay with high inward radial velocity. This efficient recycling through the galaxy itself implies that any instantaneous or quasi-instantaneous measurement of the total accretion rate of material into the galaxy will be a (possibly large) overestimate of the "net" rate of material permanently joining the galaxy by, for example, forming stars. Furthermore, this recycled material is a source of accretion onto galaxies in addition to direct cosmological accretion, which does not undergo a similar phase of processing and metal enrichment.

We are first interested in the question of whether the presence of strong galactic-scale feedback modifies the rate or character of cosmological – or "primordial" – infall. Therefore, to make a sensible comparison between simulations with and without the additional motions induced by outflows, we adopt the following approach. At any given redshift, accretion rates are measured as a tracer flux over a specific time interval, restricted to those baryons which are entering or leaving the galaxy, or its parent along the main progenitor branch, for the first time. We fix this time interval to be 250 Myr, but our results are not sensitive to this choice, so long as it is not too short to run up against the finite snapshot spacing, and not too long as to effectively smooth over changing physical conditions. In practice, we calculate three rates related to baryonic fluxes with respect to the galaxy:

(i) The outflow rate as the number of tracers with outward crossings through $0.15\,r_{vir}$ during this time window.

(ii) The raw (as opposed to net) inflow rate as the number of tracers with inward crossings across this same boundary during this time window.

(iii) The net accretion rate as the outflow rate subtracted from the inflow rate. That is, the difference of the number of tracers with inward $0.15\,r_{vir}$ crossing times and outward $0.15\,r_{vir}$ crossing times during this time window.

In each case the tracer count is then multiplied by the tracer effective mass (the initial gas cell mass divided by the initial number of tracers per cell) and normalized by the time window to derive a rate. This method gives a measurement of $\dot{M}_{gas}^{prim}(M_{halo}, z, dir, mode)$ for $M_{halo} \in [10^9, 10^{12}]\,M_\odot$, $z \in [0,5]$, $dir \in \{in, out, net\}$ and $mode \in \{all, smooth, clumpy, stripped, recycled\}$ where "prim" denotes the primordial qualification. Alternatively, in Section 6.1 we discuss another approach where the requirement on first incorporation is relaxed; instead we can calculate fluxes using the most recent incorporation time, thereby measuring a sum of material with two origins – primordial as well as having previously cycled through the MPB.

3.1 Galactic accretion as a function of redshift

In Fig. 1 we compare the net smooth accretion rate between the two simulations, restricted to haloes in the mass range $11.3 < \log{(M_{halo,tot}/M_\odot)} < 11.4$ which we keep constant as a function of redshift. At $z = 5$ the virial temperature of these haloes is $\simeq 10^6$ K, decreasing to $\simeq 10^{5.3}$ K at $z = 0$. In this box, the mass selection contains 3 haloes at $z = 5$, 42 at $z = 2$, and 53 at $z = 0$. Comparing the two simulations, we find that feedback suppresses smooth cosmological accretion
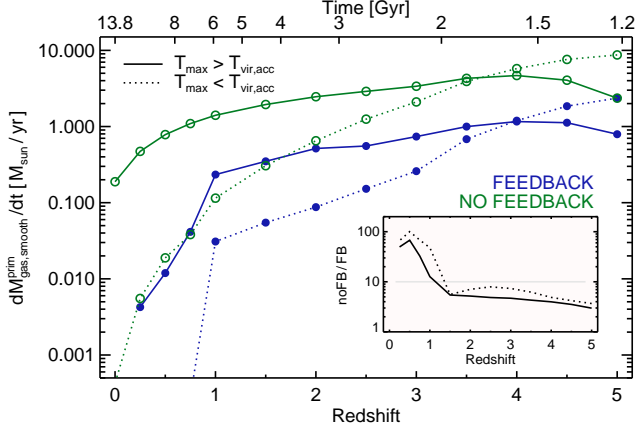
Figure 1. The net smooth gas accretion rate of cosmological origin onto central galaxies as a function of redshift. At each redshift accretion over a time window of $\Delta t = 250\,\mathrm{Myr}$ contributes. We include here only haloes in the mass range $11.3 < \log\left(M_{\mathrm{halo,tot}}/\mathrm{M}_\odot\right) < 11.4$, and separate the contribution based on the comparison of the maximum past temperature $T_{\max}$ of each Monte Carlo tracer to the virial temperature of future parent halo, at the time of accretion. Both simulations, with (blue) and without (green) our fiducial feedback implementation, indicate that relatively cold gas dominates the primordial infall onto galaxies only at redshifts $\gtrsim 4$, while at later times the reverse is true. At this mass scale, the impact of feedback is reduce the total rate of smooth cosmological accretion independent of the $T_{\max}$ comparison, by a redshift-dependent amount (see inset).

Figure 2. The smooth gas accretion rate of cosmological origin onto central galaxies as a function of redshift. At each redshift accretion over a time window of $\Delta t = 250\,\mathrm{Myr}$ contributes. We include here only haloes in the mass range $11.3 < \log\left(M_{\mathrm{halo,tot}}/\mathrm{M}_\odot\right) < 11.4$, and consider separately the contribution from net inflow, outflow, and raw accretion. The grey band indicates the upper and lower quartiles about the median for the noFB net line.

by a factor of $\simeq 3$ at high redshift ($z = 5$). This increases to $\simeq 10$ by $z = 1$ after which the suppression continues to increase towards redshift zero, while the individual net rates also steadily decline. Indeed, the net smooth accretion rates drop by roughly an order of magnitude from $z = 1$ to $z = 0$ even in the noFB run, and this drop is also evident if we consider accretion over all modes, not just smooth. The star formation rate (SFR) of haloes in this mass range declines only moderately over this same time (by a factor of ~ 2, Genel et al. 2014), implying that the component of the late time SFR in these systems supplied by smooth gas accretion is supported predominantly by material which has cycled through the direct progenitor at an earlier time.

We further split the smooth total based on the comparison between $T_{\max}$ and $T_{\mathrm{vir,acc}}$, available on a per tracer basis (as in Nelson et al. 2013). In this mass regime, the balance of these two components is similar between both runs, where at $z > 4$ gas with $T_{\max} < T_{\mathrm{vir,acc}}$ dominates the smooth cosmological accretion budget, by up to a factor of three at $z = 5$. Towards lower redshift gas with $T_{\max} > T_{\mathrm{vir,acc}}$ instead dominates, by a factor of ~ 4 at $z = 2$ and by several orders of magnitude by $z = 0$. As we discuss later in more detail, the similar balance of these two temperature components between the FB and noFB runs implies that the winds have marginal impact on the temperature history of smoothly accreting material, and that the presence of winds does not preferentially prevent material of a particular temperature history. To give a sense of reference, the difference between the mean $T_{\max}$ of cold versus hot temperature history gas is $\simeq 0.9$ dex (at $z = 5$) and $\simeq 0.6$ dex (at $z = 0$).

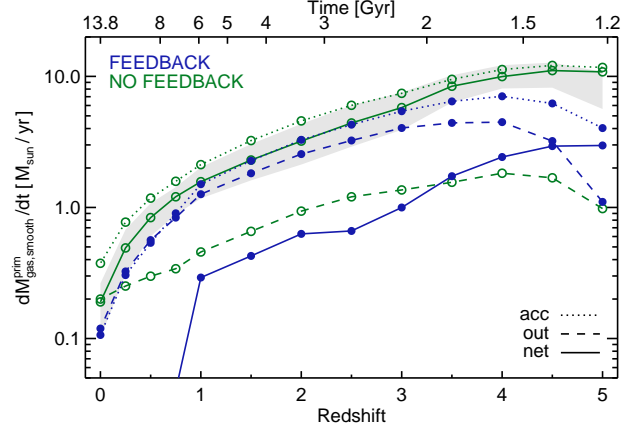To understand the declining net accretion rates towards

redshift zero, Fig. 2 shows the separate measurements of net accretion, outflow, and raw inflow, disregarding the comparison between $T_{\max}$ and $T_{\mathrm{vir,acc}}$. The "outflow" in the no feedback run arises primarily from dynamical gas motions, particularly due to galaxy-galaxy interactions. Any induced velocity which moves a tracer outside the $0.15\,r_{\mathrm{vir}}$ radial boundary will result in a non-zero outflow rate. This situation could arise during a merger or fly-by which generates any of (i) a tidal gas tail, (ii) a re-distribution of gas away from the halo centre, (iii) turbulent gas motions, (iv) or the merging companion itself passing in and subsequently out of this radius. In some sense this level of outflow represents an unrelated contribution (or noise floor) to the measurement of true, feedback induced outflows. In the case of smooth accretion, we see that this contribution is at least a factor of a few below the accretion level in the no feedback case. In the feedback run, however, large outflow rates balance about half of the inflow, this factor increasing towards redshift zero. The result is the suppression of the net smooth accretion rate at all redshifts already noted from the previous figure. Interestingly, the raw inflow rates also differ between the two runs, being suppressed in the FB case by a factor of roughly two, again at all redshifts. We find these same trends in the other accretion modes, as well as in the total accretion, disregarding mode. They also hold for all halo masses down to $\sim 10^{10.5}\,\mathrm{M}_\odot$, below which the noFB simulation begins to show a similar increase in "outflow" as we reach the limit of sufficiently-resolved galaxies.

We first consider the ratio of the net rate of the $T_{\max} < T_{\mathrm{vir,acc}}$ component to the total primordial net rate, independent of past maximum temperature, $f_</f_{\mathrm{tot}}$. This ratio declines monotonically towards redshift zero for all halo masses, such that its maximum value always occurs at the highest redshift for which a given halo mass is present in the simulation volume. We explicitly show this ratio for each mode in Fig. 3. Contrasting smooth accretion between
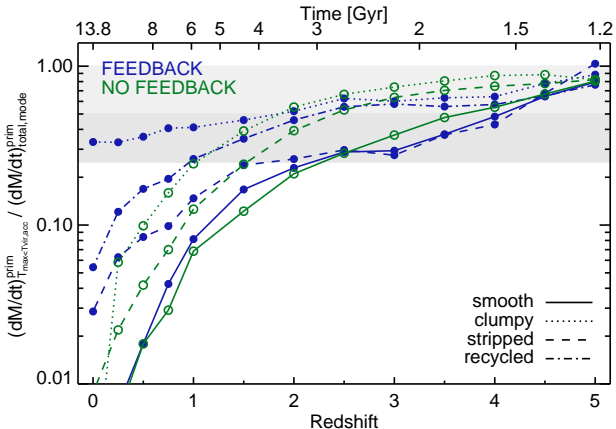
Figure 3. Ratio of accretion with $T_{\max} < T_{\mathrm{vir,acc}}$ to the total primordial rate, regardless of $T_{\max}$. We include accreted gas of cosmological origin acquired onto central galaxies over a time window of $\Delta t = 250\,\mathrm{Myr}$ as a function of redshift. The total inflow is subdivided into smooth, clumpy, stripped, and recycled components, where only gas making a net contribution to the accretion rates is included. Grey bands indicate 25%, 50%, and 100% levels.

the two runs at any given redshift we find that $f_< / f_{\mathrm{tot}}$ is nearly identical. The simulation with feedback has smaller values at high redshift ($z > 5$), and larger values at low redshift ($z < 2$), the crossover occurring between $2 < z < 3$ at all halo masses. Therefore, while feedback in these systems strongly suppresses the rate of accretion of smooth primordial gas, it does not directly affect the temperature history of this material. Although gas which flows in cold may undergo additional heating as a result of feedback, this heating is not significant enough to generally increase $T_{\max}$ above $T_{\mathrm{vir,acc}}$. Furthermore, gas which flows in hot may suffer a lower $T_{\max}$ value due to metal-line enhancement of the cooling rates, but not at a level to suppress it below $T_{\mathrm{vir,acc}}$. The first point implies that outflowing winds do not disrupt inflowing streams, at least not enough to induce mixing with the surrounding hot halo gas. Nor does the wind material itself incorporate into the streams in a way which modifies their temperature, although here our choice of low thermal energy for stellar winds may be partly responsible and potentially masking such an effect. In the following section we consider whether the presence of outflows increases the time required for gas to inflow from the virial radius to the galaxy. Here we conclude that the temperature history of gas acquired by central galaxies in a smooth mode from the intergalactic medium is largely unmodified by our fiducial feedback model.

Significantly different behaviour is seen for baryonic mass which accretes as part of a resolved substructure as it crosses the virial radius. In both the FB and noFB runs, $f_< / f_{\mathrm{tot}} \gtrsim 0.5$ for this clumpy material for all redshifts $z > 2$. This ratio drops to nearly zero towards $z = 0$ in the noFB run, indicating that material incorporated into galaxies which entered the halo bound to a satellite nevertheless experiences heating comparable to smoothly accreted gas. In contrast, this ratio only drops to $\simeq 0.4$ by $z = 1$ and $\simeq 0.35$ by $z = 0$ in the FB run. We propose that metal enrichment

in satellites prior to accretion into the MPB enables more efficient radiative cooling at later times, preventing a sizeable fraction of this gas from reaching a maximum past temperature as high as its counterpart in the noFB run. This would require a gradual heating process, such as the mixing and stripping of satellite gas during its orbit through a larger hot halo, processes which remain largely unexplored in the present work.

A similar though less prominent effect is also evident for stripped material. Recycled material – which was part of a stellar feedback driven wind at some previous time, but could otherwise be part of any accretion mode – has a redshift evolution comparable to that of stripped gas, supporting the idea that one or more epochs of metal enrichment in the ISM of an external galaxy, prior to accretion, can suppress $T_{\max}$.

3.2 Gas acquisition by the halo

It is notable that for material acquired by the halo itself this same ratio $f_< / f_{\mathrm{tot}}$ does differ between the simulations. In particular, we consider the net flux of tracers crossing $1.0\, r_{\mathrm{vir}}$ for the first time over the past 250 Myr, without necessarily also crossing $0.15\, r_{\mathrm{vir}}$. For z < 1, in the same halo mass range of $11.3 < \log\left(M_{\mathrm{halo,tot}}/\mathrm{M}_\odot\right) < 11.4$, we find $f_< / f_{\mathrm{tot}} \simeq 0.9$ in the run without feedback versus $f_< / f_{\mathrm{tot}} \simeq 0.6$ in the run including feedback. We expect this fraction to be large in both cases, since the temperature distribution of material near the virial radius is dominated by gas at temperatures lower than the virial temperature. Specifically, the median radial temperature profile of the hot halo gas at $z = 0$, $T(r)/T_{\mathrm{vir}}$, decreases with radius to a minimum of $\simeq 0.5$ at $r/r_{\mathrm{vir}} = 1$. We then expect that for most gas the ratio $T_{\max} / T_{\mathrm{vir,acc}}$ will reach a maximum of ~ 0.5 in both runs. On the other hand, the exact fraction of gas satisfying $T_{\max} \text{ ¡ } T_{\mathrm{vir,acc}}$ could be lower than unity if the gas temperature distribution at the virial radius extended into a high temperature tail.

This is not true in the FB case, implying that accreting gas has already evolved following a different temperature history prior to interaction with the halo. As a check, we make a simple measurement of the temperature of gas in the intergalactic medium, defined as all gas cells outside of all friends-of-friends groups. Between the FB and noFB runs, the IGM temperature distribution is similar at high redshift ($z > 3$) and deviates strongly by $z = 0$. In particular, while the mean IGM temperature in the noFB case remains essentially constant between $0 < z < 2$ at $T_{\mathrm{IGM}} \simeq 10^{4.2}$ K, in the FB run it increases from that value at $z = 2$ to $T_{\mathrm{IGM}} \simeq 10^{5.3}$ K by $z = 0$. The primary cause is our black hole feedback model operating in the radio-mode, which begins to alter the global IGM temperature statistics in the simulated volume as haloes of sufficiently high mass begin forming at $z \simeq 3$. In a larger simulation volume this would take place at higher redshift, and with a less homogeneous effect on the global box. We caution, however, that the gas content of massive systems is too low in our simulations (Genel et al. 2014), indicating that although the radio-mode model is efficient at moderating stellar mass growth in these haloes, its side effects – including the strong influence on IGM temperature – likely imply that the details of this model require modification.
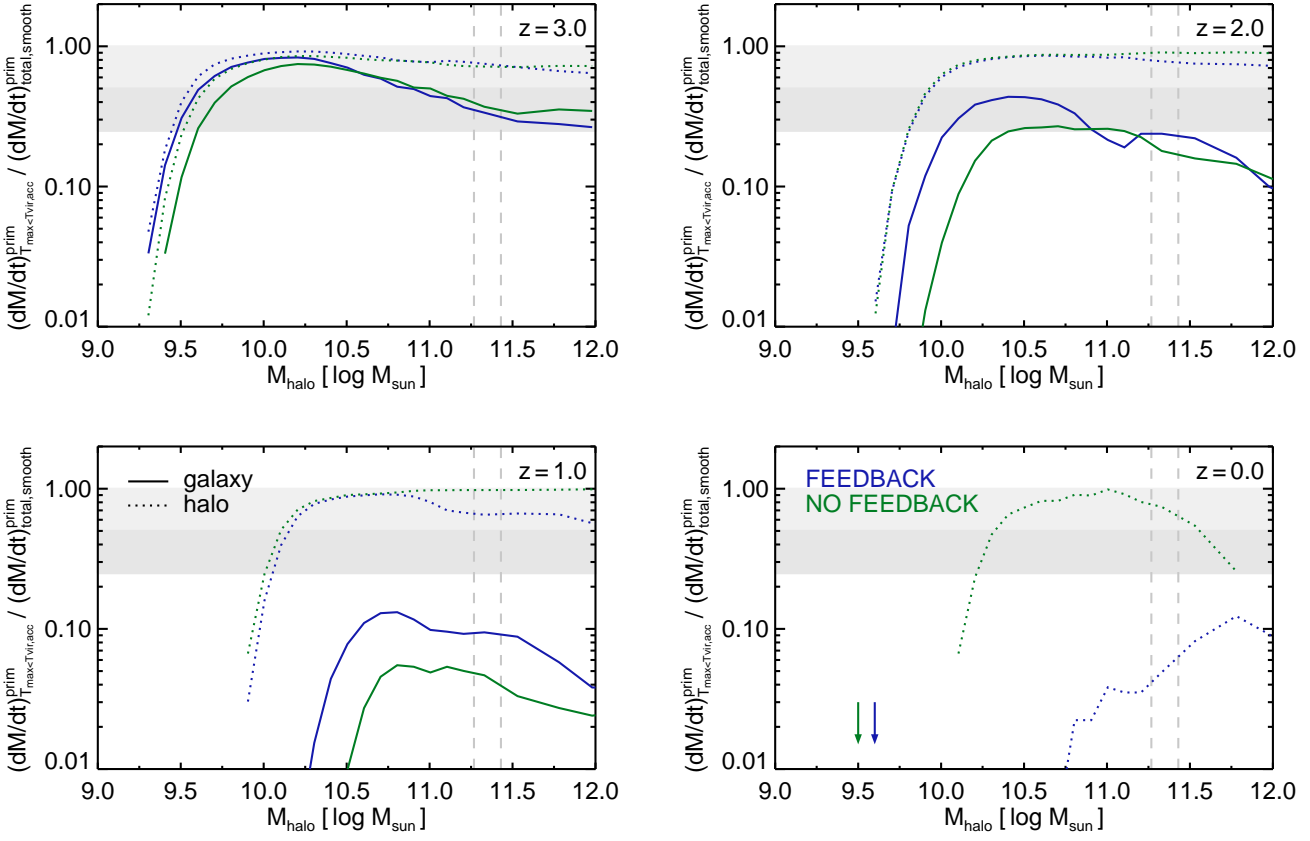
Figure 4. Ratio of accretion with $T_{\max} < T_{\mathrm{vir,acc}}$ to the total primordial rate as a function of halo mass. We include smoothly accreted gas of cosmological origin acquired onto central (solid) galaxies and their parent haloes (dotted) over a time window of $\Delta t = 250\,\mathrm{Myr}$ ending at four specific redshifts ($z \in \{0, 1, 2, 3\}$). Only gas making a net contribution to the accretion rates is included. The fractional contribution of the colder component onto galaxies evolves downward with redshift largely independent of halo mass, and similarly between the two runs. At low redshift, $z < 1$, the FB run suppresses this fraction for gas accretion onto haloes as a result of significant heating prior to crossing the virial radius. Horizontal grey bands indicate the 25%-50%, and 50%-100% levels, and dotted vertical lines indicate the mass range considered throughout.

In Fig. 4 we show how the fraction of gas with $T_{\max} < T_{\mathrm{vir,acc}}$ smoothly accreted onto haloes develops this difference between the FB and noFB cases as a function of halo mass, for four redshifts. The fraction of $T_{\max} < T_{\mathrm{vir,acc}}$ material accreted onto haloes agrees at $z = 2$ when comparing the FB and noFB runs. However, for sufficiently massive haloes by $z = 1$ this fraction is suppressed by a factor of two in the FB run, and drops to 10% or less by $z = 0$. It is notable that this same difference is *not* seen for accretion onto galaxies at low redshift. In this case, for the runs both with and without feedback, the fraction of gas with $T_{\max} < T_{\mathrm{vir,acc}}$ drops to zero at late time. This indicates that, despite the thermal history differences due to the IGM temperature, further heating proceeds within the halo before accretion onto the galaxy. The relative importance between a single strong virial shock, a series of smaller shocks within the halo, and adiabatic compression in this gas heating process remains an interesting question for future work.

3.3 Relative importance of different accretion modes

Having so far focused on smooth accretion, we now consider the importance of the different accretion modes. In Fig. 5 we show the fractional contribution of each mode to the total net accretion rate as a function of redshift. Each of the four modes is split into a separate panel. Each mode is further divided based on the comparison between $T_{\max}$ and $T_{\mathrm{vir,acc}}$. Most clearly, the contribution of smooth and clumpy accretion modes moves in opposite directions between the two runs. The inclusion of feedback physics suppresses the total relative contribution of smooth accretion by a factor of ~ 2. This is true at essentially all redshifts, and for all gas regardless of temperature history. However, the contribution of the smooth component to $T_{\max} < T_{\mathrm{vir,acc}}$ gas towards $z = 0$ is especially modified, being reduced to a negligible amount by the present day. We note that this conclusion holds without contradiction given our earlier finding from Figure 1 that the contribution of $T_{\max} < T_{\mathrm{vir,acc}}$ gas to the smooth component – that is, the "cold fraction" of smooth accretion – is largely unchanged.
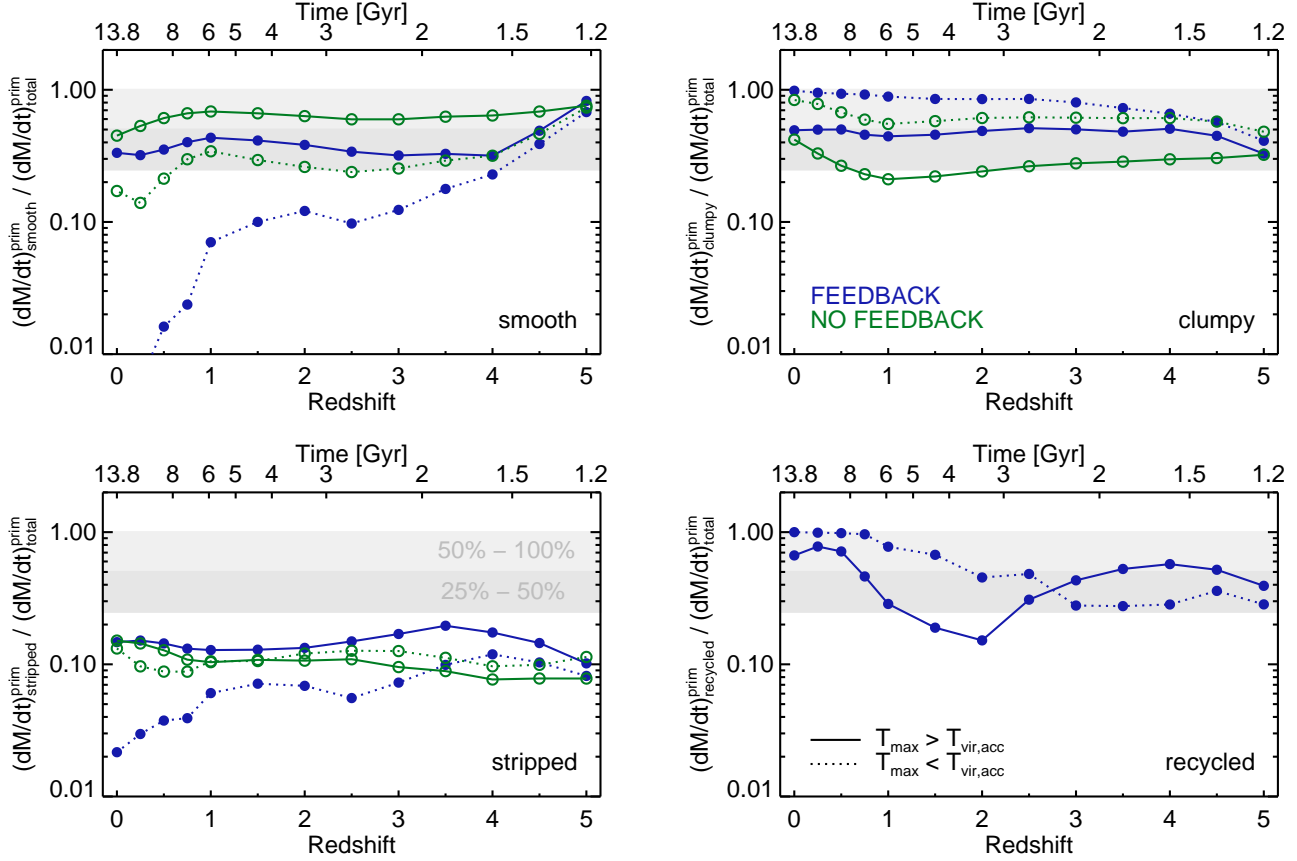
Figure 5. The fractional contribution of each accretion mode to the total net accretion rate of gas from cosmological origin onto central galaxies over a time window of $\Delta t = 250\,\mathrm{Myr}$, as a function of redshift. We separate the contribution based on the comparison of the maximum past temperature T_{max} of each Monte Carlo tracer to the virial temperature of future parent halo, at the time of accretion. The grey band indicates the 25% to 50% range. The four modes are smooth, clumpy, stripped, and recycled. The feedback run decreases the fractional importance of smooth accretion, regardless of temperature history and for all redshifts, particularly for cold material at late times.

The fractional importance of stripped material is similar between the two runs. By definition the hot and cold component lines both sum independently to one (excluding recycled, which is an additive attribute). Consequently, the contribution of resolved substructures increases to balance the decrease of the smooth mode. In terms of primordial accretion contributing to the net growth of galaxies, for most of cosmic time, $z < 3$, more than 80% (less than 40%) of material with a cold (hot) temperature history is acquired in the clumpy mode. This exact fraction will be sensitive to the definition of substructure – for instance, we include the entirety of a satellite halo, whereas Kereš et al. (2009) includes only the actual satellite galaxy/ISM material. Finally, tracers which have at some point in their past resided in the wind phase make up a significant fraction of the total net rate, particularly at late times – redshift zero growth is dominated by this recycled component. However, the fact that we are here only considering gas which has entered the MPB for the first time implies that this is largely recycling in satellite systems prior to incorporation into the central galaxy.

4 THE STATE OF GAS IN THE HALO

Here we consider the instantaneous properties of gas flows in the halo regime, regardless of its past or future history. To begin, Fig. 6 shows a prototypical, single halo in the mass range under consideration, matched between the two runs, at $z = 2$. An orthographic projection with extent in all dimensions equal to 3.5 times the virial radius (indicated with the largest white circle) shows gas density, mass-weighted gas temperature, and mass-weighted gas radial velocity, where negative denotes inflow. The run without feedback is shown on the top row, while the run with feedback is shown on the bottom row.

The temperature projection reveals that the energy injection from feedback arising in the central galaxy pushes the hot halo gas to slightly larger radii. The existence of cold and metal enriched wind material in our model suppresses the peak temperature in the inner halo, both directly and due to enhanced cooling. The stellar feedback driven winds clearly populate the inner halo ($r/r_{\mathrm{vir}} < 0.5$) with a large mass of cold gas with high covering fraction, substantially altering the temperature and velocity structure of gas at these small radii. Further from the galaxy, we see that
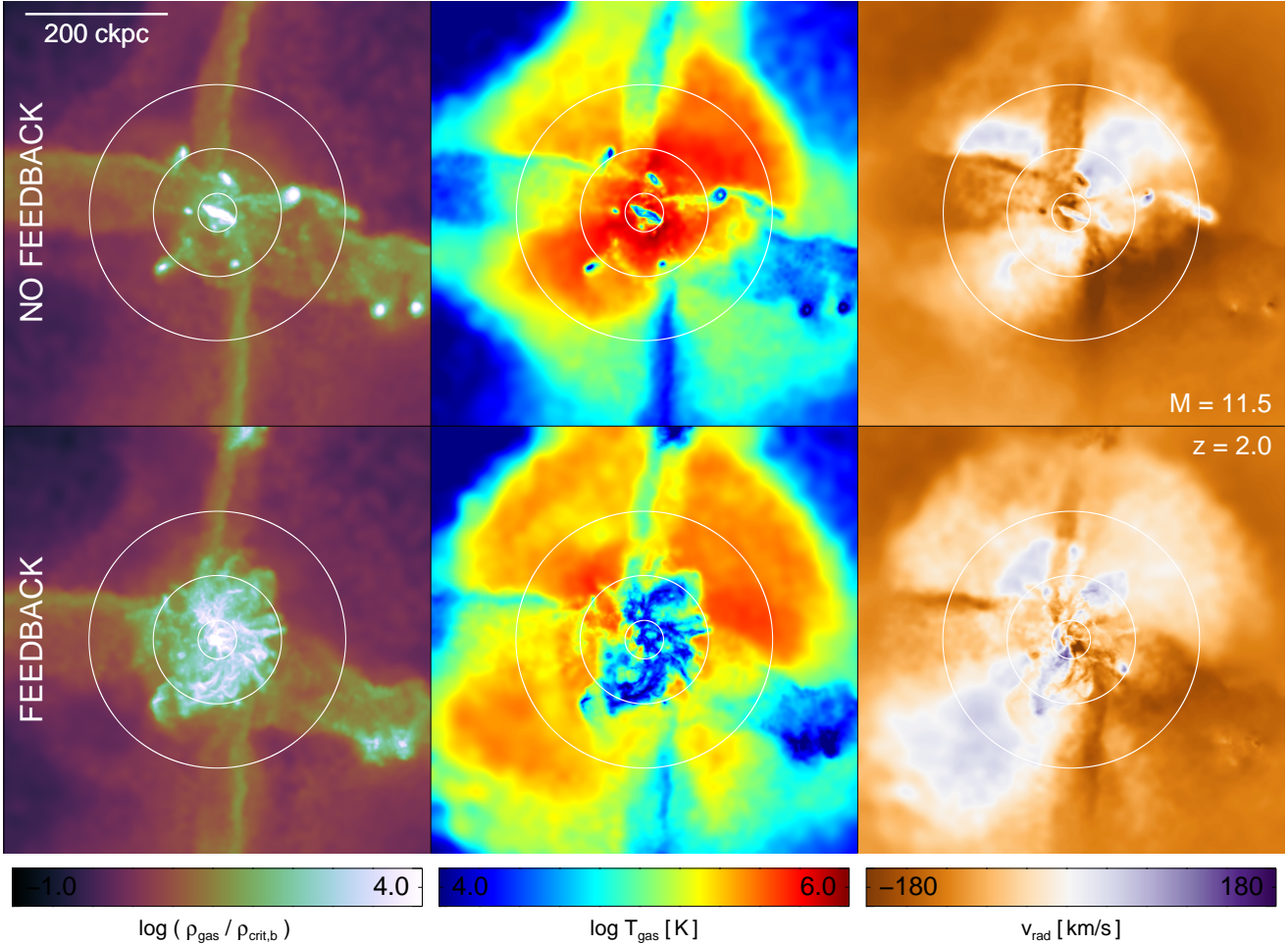
Figure 6. Comparison of a single halo with a mass of $10^{11.5}\,\mathrm{M_\odot}$ at $z = 2$ between the FB and noFB runs. Shown in projection are gas density (left), mass-weighted temperature (middle), and mass-weighted radial velocity (right). The three white circles are the same in all panels and denote $[1.0, 0.5, 0.15]\, r_{\mathrm{vir}}$. Negative v_{rad} (brown) is infall, whereas positive (purple) v_{rad} is outflow. Introducing the feedback model pushes the hot halo gas to larger radii, while increasing the fraction of the virial sphere covered by outflow. Gas streams inflowing across the virial radius are largely unaffected, in terms of their temperature, density, or radial velocity. The virial radius of this halo is 180 kpc comoving, and the virial temperature is $\simeq 10^6$ K.

more of the halo volume – and halo gas mass – is occupied by material with outward radial velocity. However, at the virial radius, gas inflow appears largely unaffected by the introduction of our fiducial feedback model. While in mass-projection the streams crossing r_{vir} appear somewhat more collimated, slower, and warmer, this is predominantly a side effect of this particular visualization. If we instead inspect spherical slices of gas properties at the virial radius, we find that there is e.g. no notable difference in the temperature distribution of inflowing material.

To be more quantitative, we construct spherical slices for all haloes at all analysis redshifts at a number of radii. We use a mass-weighted tophat kernel to interpolate gas quantities onto equal area pixels using the Healpix scheme (Górski et al. 2005). In Fig. 7 we calculate a spherical covering fraction of inflow or outflow as the fraction of pixels on this sphere with radial velocity above some threshold with the appropriate sign. As a threshold we take 10% of $v_{\mathrm{circ}}(\mathrm{r})$ of an NFW halo of equal mass. Our results are insensitive to this choice provided it is small enough – we also considered a constant threshold of $\sim 20\,\mathrm{km\,s^{-1}}$, and a threshold of zero.

The top panel shows the behaviour across the quarter virial sphere, while the bottom panel shows the same across the full virial sphere. In all cases we exclude all gas bound to resolved substructures prior to this calculation.

At $0.25\,r_{\mathrm{vir}}$, the impact of feedback is to substantially reduce the spherical covering fraction of inflow from 80%-90% down to 50%-60%, while outflow correspondingly covers more than half of the surface at $z \sim 2$–3, up from $\simeq 20\%$. At the virial radius, both runs agree that $\geqslant 70\%$ of the virial sphere is covered by inflow, regardless of redshift. In the FB case, somewhat more material has outward radial velocity at high redshifts, but for this halo mass regime the difference is small and disappears towards $z = 0$. In agreement with the single halo shown previously in Fig. 6, we see that at $z = 2$ feedback introduces a negligible change to the spherical covering fractions of both inflow and outflow at the virial radius.

In Fig. 8 we calculate the radial mass flux rate of gas across the same two radii, for both inflow and outflow, with substructures removed. Since inflow and outflow occupy disjoint portions of each sphere, these rates are in principle in-
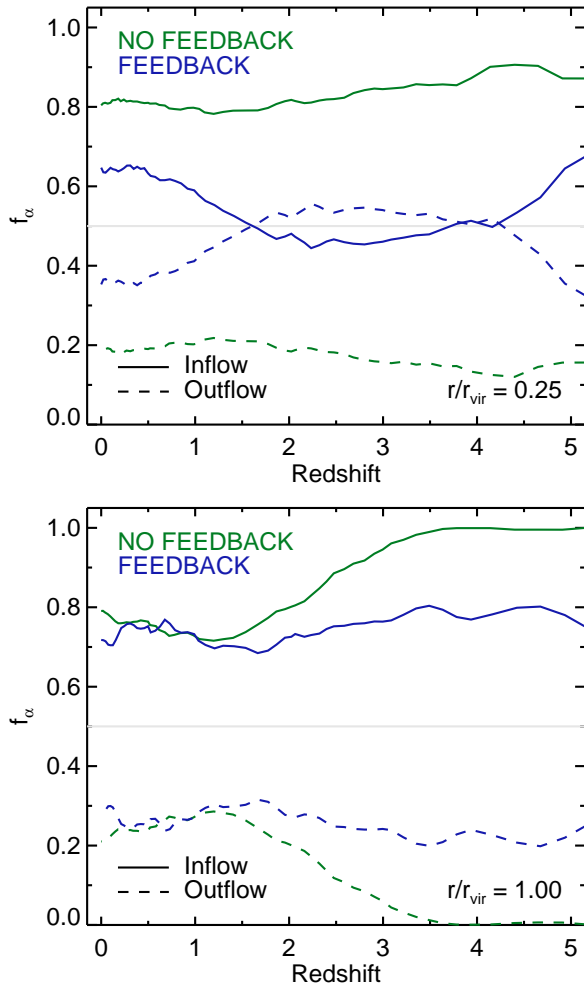
Figure 7. The spherical covering fraction of the quarter virial sphere (top panel) and full virial sphere (bottom panel) of inflow and outflow. Each is calculated as the fraction of the surface covered by gas of either positive or negative radial velocity which exceeds a relative threshold of 10% of the circular velocity of an NFW halo at that radius. Gravitationally bound substructures have first been removed. The halo mass range of $11.3 < \log{(M_{\mathrm{halo,tot}}/M_\odot)} < 11.4$ is included. Near the galaxy, the presence of feedback increases the covering fraction of outflow above half, while at the virial radius this same behaviour is seen to a lesser degree and only at high redshift.
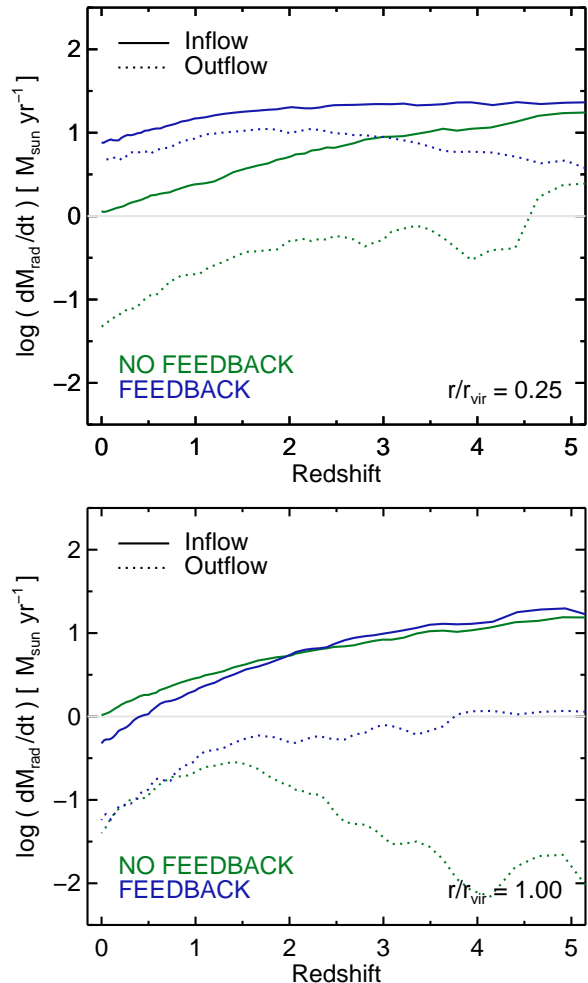
Figure 8. The radial mass flux rates across the quarter virial sphere (top panel) and full virial sphere (bottom panel), calculated separately for inflow and outflow. As in the previous figure, gravitationally bound substructures have first been removed, and the halo mass range of $11.3 < \log{(M_{\mathrm{halo,tot}}/M_\odot)} < 11.4$ is considered. While the rate of inflow across the virial sphere is unchanged, the rates of both inflow and outflow closer to the central galaxy are both significantly increased, implying recycling occurring across the $0.25\,r_{\mathrm{vir}}$ boundary.

dependent, and do not necessarily correlate with the respective spherical covering fractions. At the virial radius (bottom panel) we see that the rate of gas inflow is unchanged, while feedback boosts outflow rates at high redshift substantially, although to magnitudes which are still small relative to inflow. This outflow across the virial sphere transfers mass, and therefore metals, from within virialised haloes out into the intergalactic medium. Notably, the presence of feedback does not lower the instantaneous inflow rates, which would indicate a direct impact on the accretion of intergalactic material onto the halo. Nor does it increase the inflow rates, which would indicate large-scale recycling motion across the host halo virial radius. At $0.25\,r_{\mathrm{vir}}$ (top panel) feedback has a larger impact, increasing the rates of both inflow and out-

flow, the magnitude of the difference growing with time. Given that the fraction of this surface covered by inflow is actually smaller in the FB run, this is a clear signature of significant gas recycling motion across this boundary.

5 TIMESCALE OF GAS ACCRETION

In the previous section we saw that the morphology of inflow at the virial radius is largely unchanged. Here, we consider whether the presence of outflows increases the time required for gas to inflow (or "transit") from the virial radius to the galaxy. We measure this quantity as the time difference between the first virial radius crossing t_{halo} and the first incorporation into the galaxy t_{gal}. In Fig. 9 we show the distribution of this time difference for all tracers within haloes
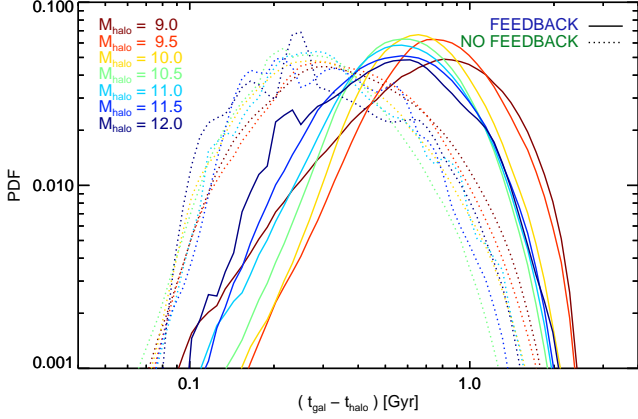
Figure 9. Distribution of time difference between the first $1.0\,r_{\rm vir}$ and $0.15\,r_{\rm vir}$ crossings (the "halo transit time" for each tracer during its first accretion into the halo) for smooth accretion only. Includes all tracers within haloes which have recorded these two crossings by $z = 2$. Separated by halo mass (colored lines) and for the no feedback (dotted) and feedback (solid) runs. The FB run shifts each distribution, regardless of halo mass, to longer times by a constant factor of ~ 2-3. In addition, for both simulations, the distribution of transit times is nearly independent of host halo mass.

at $z = 2$ which have previously recorded these two crossing times, split into halo mass bins from $10^9\,{\rm M}_\odot$ to $10^{12}\,{\rm M}_\odot$. We include only smooth accretion.

First, in both runs and for all halo masses we find a broad, uni-modal distribution. That is, there is no obvious evidence for multiple channels of accretion having different halo crossing timescales. Comparing the FB (solid) and noFB (dotted) runs, we find that feedback introduces a significant delay in the halo transit time of smooth mode material. Each distribution shifts to longer times by a factor of ~ 2-3, and this factor is largely independent of halo mass, at least above $10^{10}\,{\rm M}_\odot$, where systems are well resolved. Specifically, gas smoothly accreted by $z = 2$ takes on average $\simeq 250\,{\rm Myr}$ to cross from the virial radius to the galaxy in the noFB run, and $\simeq 700\,{\rm Myr}$ in the FB run.

Of even more interest, we see that in both simulations, this halo transit time is again largely independent of halo mass. This implies that this time difference may be related more to the dynamical time and *not* to the cooling time, since the latter scales strongly with halo mass. Over the halo mass range of $10^{10}\,{\rm M}_\odot$ to $10^{12}\,{\rm M}_\odot$, then, we see no evidence for a transition point above and below which the process of gas accretion through the halo occurs in a fundamentally different way, at least insofar as is captured by our measured "halo transit time". We return to this point and its implication for the idea of a critical halo transition mass in the discussion.

To further explore any possible relationship between this transit time and different accretion mechanisms, Fig. 10 shows the relation with the $T_{\max}$ of each tracer. The question is whether or not gas with low $T_{\max}$ has a shorter halo transit time, while gas with higher $T_{\max}$ spends longer in the halo, as might be naively expected. We see a weak correlation in this direction for the noFB simulation (bottom panel), which is less clear after including feedback (top panel). This lack of
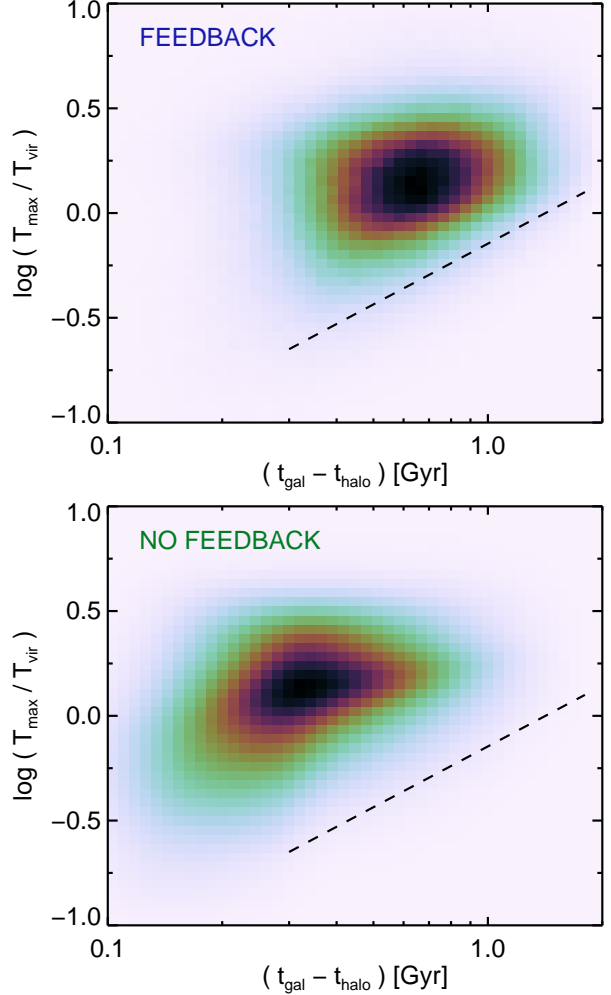

Figure 10. Correlation between $T_{\max}$ and "halo transit time" ($t_{\rm gal}$-$t_{\rm halo}$), where the colour scale indicates the mass distribution of tracers smoothly accreted by $z = 2$ in this plane. While the noFB run (bottom panel) may indicate a relation between maximum past temperature and halo transit time, this is less clear in the FB run (top panel). In both cases there is a lower envelope, approximately indicated by the dashed line in the top panel, indicative of a minimum $T_{\max}$ which increases with increasing transit time.

correlation implies that the mean halo transit times for both hot and cold gas are comparable. That is, there is no strong signature of the past thermal state of gas in its dynamical history, at least insofar as is measured by the halo transit time. In both simulations, notably, there is clearly a lower envelope. This is indicated in the top panel by the dashed black line, which shows the relation

$$\log\left(\frac{T_{\max}}{T_{\rm vir,acc}}\right) = \frac{(t_{\rm gal} - t_{\rm halo})}{2\,{\rm Gyr}} - 0.8. \tag{1}$$

We see that gas does not populate the region to the lower-right of this relation – that is, there is a minimum $T_{\max}$ reached which increases as a function of increasing halo transit time. Note that we have here stacked together haloes of all masses, but we see this relation also when we examine
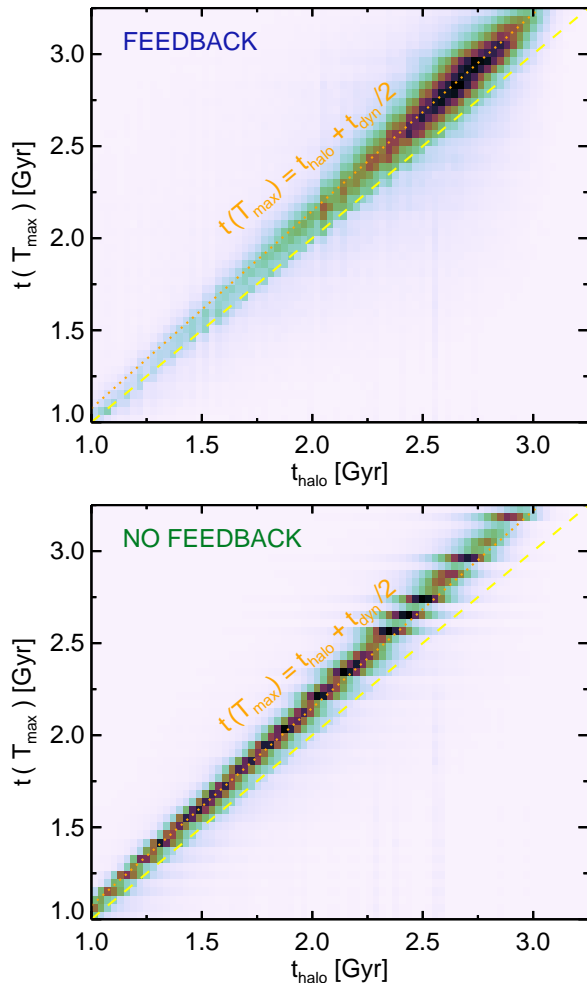
Figure 11. The tracer mass distribution in the plane of $t(T_{max})$, the time when the maximum past temperature was obtained, and t_2, the time of first virial crossing. Both are given in terms of the age of the universe, where the yellow dashed line shows the 1-to-1 relation. The orange dotted line is offset by a constant factor, such that tracers on this relation would have reached their maximum temperature a time $t_{dyn}/2$ after crossing the virial radius. Smooth accretion only, for tracers which have entered haloes by $z=2$.

small bins in halo mass. This implies that there is at least some link between virial heating and the gas dynamics of accretion. We therefore want to understand where the maximum temperature of each tracer is reached – is the T_{max} event closely related to the virial crossing time, or does it occur on average with either a positive or negative relative lag.

In Fig. 11 we show the correlation between the time of T_{max} and the time of the first virial radius crossing, both in terms of the age of the universe, on a tracer by tracer basis. Only smooth accretion is included. The yellow dashed line shows the 1-to-1 line, which would imply that gas heats at r_{vir} to its maximum temperature, subsequently cooling in order to join the ISM of the galaxy. The dotted orange line shows a constant positive time offset of $t_{dyn}/2$ later, where we take the redshift dependent
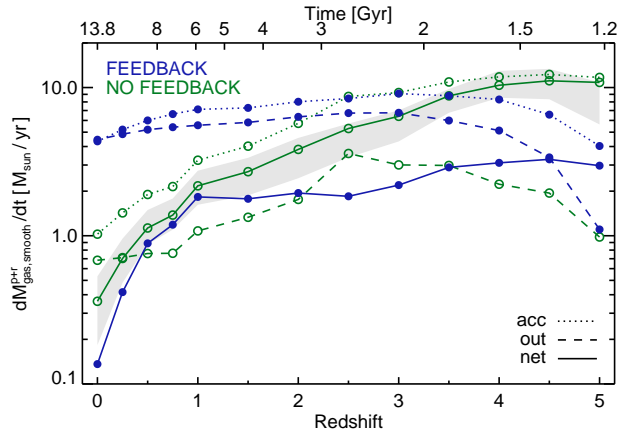

Figure 12. As in Fig. 2 but showing the combined smooth gas accretion rate, including both primordial and material previously cycled through the main progenitor branch. We include accretion onto central galaxies as a function of redshift. As before, we include only haloes in the mass range $11.3 < \log(M_{halo,tot}/M_\odot) < 11.4$, and consider separately the contribution from net inflow, outflow, and raw accretion.

$$t_{dyn} = r_{vir}/v_{circ}(r_{vir}). \qquad (2)$$

In both runs, these two lines bound the majority of accreted material, implying that gas reaches its maximum temperature shortly *after* first accretion into the halo, and never before. It is clear that the ratio $t(T_{max})/t_{halo}$ increases with time, but since t_{dyn} also evolves with redshift, becoming longer at later times, we can see that the characteristic lag time is $\simeq 0.5\,t_{dyn}$, at least for all accretion which has occurred by $z=2$. Comparing the two panels, we conclude that the relation between heating and virial crossing for smoothly accreted gas is not strongly affected by the presence of our fiducial feedback model. This result holds also for accretion taking place by $z=1$ and $z=0$, although the mean lag time increases to $\simeq 1.0\,t_{dym}$ for gas entering the halo at late times $(z<1)$.

6   DISCUSSION

6.1   The contribution of recycled gas

We have so far focused exclusively on the accretion of material of primordial, or cosmological, origin. We can contrast this evolution of $\dot{M}_{gas}^{prim}$ from Section 3 with the fundamentally different net accretion rates obtained if we count tracers with *most recent* incorporation times, as opposed to *first* incorporation times, within the past 250 Myr. We denote this measurement $\dot{M}_{gas}^{p+r}$, where the combined contributions from primordial and material previously cycled through the MPB are two disjoint subsets of accretion which sum to the total instantaneous accretion rate. As a result, this measurement includes all gas motion across the boundary defining the galaxy, regardless of when that gas initially entered the galaxy. Note that by definition, tracers within the galaxy with outward crossings are a strict subset of tracers within the galaxy with inward crossings. They represent the mass component which cycles out of, and back into, the galaxy during the 250 Myr time interval.

Fig. 12 revisits the smooth accretion rate as a function of redshift, where the relationship between the FB and noFB runs is significantly altered when compared to Fig. 2. As expected, inflow and outflow rates are higher for both runs at low redshift. The scaling of inflow rates with redshift in the noFB run remains similar, with the net accretion rate declining monotonically from $z \simeq 3$ to $z = 0$. However, the inclusion of feedback maintains a nearly constant net accretion rate until $z = 1$. The smooth "p+r" accretion rate at high redshifts, $z > 4$, is similar to the primordial accretion only value, implying that the contribution of recycled gas is negligible at early times. However, recycling becomes more important towards low redshift, at a level sufficient to balance the decreasing inflow of primordial gas. Between $z = 1$ and $z = 0$ the raw inflow rates decrease by factor of ~ 2 in both simulations, pulling the net acquisition of smooth mode material down by a similar factor.

We can also reconsider the ratio of accretion with $T_{\max} < T_{\mathrm{vir,acc}}$ to the total rate, as in Fig. 3, but including the recycled component (not shown). In the feedback run, the fraction of material with $T_{\max} < T_{\mathrm{vir,acc}}$ is larger at all redshifts. In particular, at $z = 0$, the ratio to the total is $\simeq 0.04, 0.15, 0.25$ and 0.4 for smooth, stripped, recycled and clumpy modes, respectively. The greater fraction of accretion with a cold temperature history reflects a simple time preference – that recycled gas on average enters the halo earlier than non-recycled gas, combined with a cold fraction which increases towards higher redshift.

The other interesting difference we find when including the recycled component in our analysis appears in the fractional contribution of each accretion mode to the total net rate, as in Fig. 5. In this case, the conclusions for hot material with $T_{\max} > T_{\mathrm{vir,acc}}$ are all qualitatively unchanged, whereby feedback still suppresses the relative importance of smoothly accreted gas by a similar amount. However, for colder material ($T_{\max} < T_{\mathrm{vir,acc}}$) the fraction contributed by each of the smooth, clumpy and stripped modes converges to similar values for the FB and noFB runs. The reason remains somewhat unclear, and may be coincidental. As expected, the recycled mode also becomes more significant, since we now include recycling within the main progenitor branch. In this case, the contribution is monotonically increasing towards low redshift, increasing from $z = 5$ to $z = 0$ from 0.3 to 1.0 (cold) and from 0.6 to 1.0 (hot). That is, by redshift zero, essentially all gas being accreted by galaxies in this mass regime has been previously recycled at least once.

An in-depth consideration of the recycled mode is beyond the scope of this paper, and remains a topic for future work. Of particular interest is the recycling timescale – that is, the amount of time between ejection in a wind and re-incorporation into a galaxy. This quantity is particularly important in semi-analytic models, for instance to fix the overly early build-up of low mass galaxies (Henriques et al. 2014). Further, our analysis methodology, which revolves around recording only one radial crossing time per direction per radius per tracer, implicitly assumes that gas does not cycle through the same radius more than once over the time interval (250 Myr). Oppenheimer et al. (2010) found, for instance, a recycling time of $\sim 1\,\mathrm{Gyr}$ at $z = 1$ for haloes of this mass. Also of interest is the prevalence of multiple recyclings, or, the number of times a baryon mass element has belonged to a wind in its history. Similarly, the contri-

bution of satellite recycling and satellite winds in general as a contributor to both the intergalactic medium and the circumgalactic medium of larger host haloes.

However, the process of recycling involves the complex wind physics associated with feedback as well as the difficult numerical problem of multiphase gas interaction (Agertz et al. 2013; Sarkar et al. 2014). More faithful modelling of stellar feedback processes and/or higher resolution than is currently available in full cosmological volumes is likely required before the process of recycling can be better understood (Hopkins et al. 2014; Aumer et al. 2013; Stinson et al. 2013; Faucher-Giguere et al. 2014; Agertz & Kravtsov 2014; Ceverino et al. 2014). In more massive haloes, treatments of AGN feedback will also need to be improved (Wurster & Thacker 2013; Costa et al. 2014; Bachmann et al. 2014; Li & Bryan 2014), while the contribution from other outflow mechanisms such as cosmic rays (Booth et al. 2013; Hanasz et al. 2013; Salem & Bryan 2014) is potentially also critical. Clearly, the baryon cycle in its entirety cannot yet be satisfactorily understood given the current level of sophistication of feedback modelling in cosmological simulations.

6.2 Implications for a critical halo transition mass

In all semi-analytic models of galaxy formation (e.g. White & Frenk 1991; Croton et al. 2006; Bower et al. 2006, and more recent efforts), a foundational theoretical consideration is the cooling of hot halo gas. This essentially governs the growth of the cold mass reservoir of the galaxy, and so the subsequent star formation and stellar mass growth. A common approach is to let the hot halo gas with $t_{\mathrm{cool}} < t_{\mathrm{dyn}}$ or $t_{\mathrm{cool}} < t_{\mathrm{H}}$ cool onto the central galaxy.

Furthermore, they generally implement a critical halo transition mass, below which hot halo cooling proceeds in a "rapid" mode, and above which cooling proceeds in a "slow" mode, where the gas fraction eligible to cool drops to zero. This difference in the behaviour of quasi-static hot halo gas between more and less massive dark matter haloes is motivated largely from the classic, analytical arguments of Silk (1977); Rees & Ostriker (1977); White & Rees (1978). Analytic arguments supported by one-dimensional, spherically symmetric calculations, cast in terms of whether or not a stable virial shock can exist (Birnboim & Dekel 2003; Dekel & Birnboim 2006) have also identified a transition point in halo mass. They find that haloes below $\sim 10^{11}\,\mathrm{M}_\odot$, independent of redshift, cannot provide enough post-shock pressure to support a virial shock against losses from radiative cooling.

In Section 5 we found that for both simulations, with and without feedback, the time taken by baryons to transit from the virial radius to the central galaxy is independent of halo mass (see also Brook et al. 2014). This holds true, at the very least, for haloes with $10^{10}\,\mathrm{M}_\odot < \mathrm{M}_{\mathrm{halo}} < 10^{12}\,\mathrm{M}_\odot$. This indicates that, in contrast to analytic expectations, we see no strong evidence in the simulations for a sharp halo transition mass, above and below which the process of gas accretion proceeds in a fundamentally different manner. It will be important to validate this result in the future by extending the dynamic range of this analysis to more massive haloes. In particular, good sampling is available up to $10^{14}\,\mathrm{M}_\odot$ in the $\simeq (100\,\mathrm{Mpc})^3$ volume of Illustris.

The agreement between theoretical cooling models and

hydrodynamic simulations has been an occasional subject of interest over the past decade (Yoshida et al. 2002; Viola et al. 2008; Lu et al. 2011; Monaco et al. 2014), where the general conclusion has been that the cooling models implemented in SAMs provide an acceptable match to simulations. However, these studies have all used the smoothed particle hydrodynamics (SPH) technique, and (as Monaco et al. (2014) points out) in Nelson et al. (2013) we found that numerical inaccuracies in "classic" SPH strongly affect the processes of gas accretion in cosmological simulations, particularly failing to accurately capture the cooling properties of hot haloes. The very fact, then, that older SPH simulations agree with classic hot halo cooling theory points to a looming disagreement between that theory and modern, cosmological simulations. Understanding in what ways these simple theoretical arguments agree with numerical calculations (see also Dekel et al. 2013), and how the picture of hot halo cooling in semi-analytical models can potentially be improved upon, remains an open, important question for future work.

6.3 Comparison to previous studies

As pointed out in the introduction, reconciling previous conclusions is complicated by a variety of different feedback implementations, numerical methods, halo mass regimes, statistical samplings, and interpretations. We compare our findings with those works which specifically focused on the impact of feedback on cosmological gas accretion.

In particular, Oppenheimer et al. (2010) considered a few variations of kinetic wind schemes similar to the one presented herein, with constant velocities or a momentum-driven scaling, and decomposed star formation rates into three distinct modes: hot, cold and wind (recycled). Contrasting recycled versus non-recycled, they concluded that accretion is dominated by recycled gas below $z < 1$ for $M_{\mathrm{halo}} > 10^{11}\,M_{\odot}$, neglecting AGN effects. This is qualitatively consistent with our findings and Figure 5 for primordial accretion. They further claimed that outflows efficiently suppress both cold and hot modes, where these are defined with the standard $T_{\max}$ criterion, excluding all gas ever belonging to a wind. Our definition of primordial is different, in that it allows for recycling in satellites prior to incorporation into the MBP. Given this caveat in the comparison, our findings in Fig 1 are also qualitatively consistent with this conclusion.

Faucher-Giguère et al. (2011) also considered kinetic wind models, with various constant velocities and mass loading factors, and measured accretion rates separated into cold and hot modes based on instantaneous mass fluxes through radial shells together with instantaneous gas temperatures. In this respect the analysis differs significantly from Lagrangian definitions of accretion and thermal history, and so is not quantitatively comparable. It furthermore prohibits the identification of recycled material as in Oppenheimer et al. (2010) and this work. They focused only on flux through the virial shell (accretion onto the halo as opposed to the galaxy), and showed galaxy fluxes only for simulations with no winds. Nonetheless, neglecting AGN effects, they found that the net cold gas accretion rate onto low-mass haloes was suppressed, while the effect in high-mass haloes was negligible. Specifically, for the halo mass

range considered here, the decrease is between zero and a factor of a few, relatively independent of redshift, which is tension with the changing balance of hot versus cold accretion onto halos found in our Figure 4, and likely a result of the different wind velocity parametrisation.

van de Voort et al. (2011a) considered many simulations with different feedback physics. They found that while the gas accretion rates onto haloes was relatively robust against the presence of feedback, the rates onto galaxies themselves depended sensitively on stellar winds as well as metal-line cooling. In particular, at our halo mass scale at $z = 2$, there was negligible change in the total smooth accretion rate onto galaxies between their reference and no feedback models, although this is a sensitive function of mass. However, they also found an order of magnitude decrease in total smooth rates introducing either a density dependent wind scaling or thermal AGN feedback. The balance of hot and cold smooth accretion onto galaxies at both $z = 2$ and $z = 0$ was found to be fairly insensitive to feedback, in qualitative agreement with our findings. Their AGN model did not alter the cold fraction of smooth accretion onto haloes at $z = 2$, in disagreement with our Figure 4. As an extension, van de Voort et al. (2011b) focused on the impact of AGN feedback on inflow and found that it preferentially prevented hot mode gas, with high maximum past temperature, from cooling from the halo onto the galaxy. That is, AGN feedback reduces hot halo accretion more than cold accretion, based on analysis of all resolved haloes, although this is presumably an important effect only in massive haloes above $\simeq 10^{12}\,M_{\odot}$. We do not find this differential effect at fixed halo mass, although in this work we have focused on lower mass systems not dominated by AGN effects.

Woods et al. (2014) includes a combined delayed cooling supernova and early stellar feedback model, a numerically distinct mechanism for generation of galactic-scale winds from those just discussed. They found strong recycling, as we do. Contrasting weaker to stronger stellar feedback, they concluded that the total gas accretion rates did not change with strong feedback, while the balance between cold and hot components did. In particular, that the cold component became more important. Comparing to our results for smooth accretion, this result is in qualitative disagreement. However, this work did not differentiate the merger contribution, and concludes that more cold gas is available for accretion in strong feedback runs because more cold gas is present in satellite haloes, not due to any change in accretion processes. This could be interpreted as tentative agreement with our conclusion that the fractional contribution of clumpy accretion to the net cold rate is larger in the run with feedback (upper right panel of our Figure 5).

Finally, Übler et al. (2014) implements a hybrid thermal/kinetic stellar feedback scheme, considering five haloes slightly more massive than those discussed herein. They found that strong outflows generate substantially higher raw accretion rates, and that recycled material dominates galactic gas accretion at $z < 1$, in good qualitative agreement with our results. They also found that the strong feedback case actually increased the rate of "first" (our "primordial") gas accretion, without differentiating between thermal history or different modes. The cause is likely then related to the merger contribution, as above, with similar conclusions.

However, all six studies discussed this far have been con-

ducted with the "classical" density formulation of smoothed particle hydrodynamics (SPH, see Springel et al. 2005). They therefore agree in their "no feedback" cases with Kereš et al. (2009), finding that the cold mode dominates the accretion rates, and/or the star formation rates, of galaxies of all masses, particularly so at the higher redshifts of $z = 3$ or $z = 2$. However, we have previously shown that this result is incorrect and a consequence of numerical issues with the hydrodynamical method of SPH (Nelson et al. 2013). Moreover, as typically employed in galaxy formation simulations, SPH is not strictly numerically convergent (Zhu et al. 2014). As a result, it is somewhat unclear how to interpret any subsequent conclusions based on the inclusion of further baryonic feedback processes.

Dubois et al. (2012a) investigated AGN feedback at high redshift ($z = 6$) in a single massive halo ($10^{15}\,\mathrm{M_\odot}$ at $z = 0$), and found that large-scale hot superwinds could morphologically disturb cold filaments and quench cold diffuse accretion. This is a substantially different mass scale than the one probed here and we cannot make any direct comparison.

It has been pointed out that details of the wind interaction, travel extent, IGM enrichment, as well as its recycling properties, the balance between inflow and outflow fluxes, and the timescale of reincorporation may all be sensitive to physical model inputs as well as numerical details (Oppenheimer et al. 2010). Furthermore, current models designed to incorporate feedback and other physical effects from AGN are diverse and relatively unsophisticated, at least as applied in cosmological volumes. Finally, different analysis methodologies can make straightforward comparison between simulations impossible. While the studies discussed above seem to agree on several qualitative conclusions, it would seem premature to claim any strong agreement between simulations as to the impact of feedback on cosmological gas accretion. To do so would require identical analysis techniques applied to either large volumes with statistically robust galaxy populations, or identical initial conditions of individual haloes, with equivalent physical models and numerical implementations for non-feedback physics, including stellar evolution, metals, cooling, star formation, ISM pressurisation, hydrodynamics, and gravity. All of the studies reviewed here differ in one or more of these aspects, motivating a more controlled investigation in order to resolve this question.

7   CONCLUSIONS

In this paper we have compared two simulations, realisations of the same initial conditions evolved with the moving mesh code AREPO, using the same methods for both gravity and hydrodynamics. One, which we label as "no feedback", includes only the simplest baryonic physics – radiative cooling of a primordial gas, and star formation. The other, which we label as "feedback", implements the full physics model of the Illustris simulation project, with all models and parameters unchanged. Most importantly, the latter includes metals and metal-line cooling from enriched gas, stellar feedback resulting in galactic-scale winds, as well as feedback from supermassive black holes. This model has been shown to successfully reproduce a number of key stellar observables,

in particular the $z = 0$ stellar to halo mass relation, and the star formation rate density as a function of redshift, over the full halo mass range we consider here. Our aim was to understand how such a comprehensive set of feedback processes, implemented in a full cosmological volume, affects the mechanisms by which galaxies acquire their baryonic material. Focusing on the accretion of gas by galaxies over cosmic time, we have arrived at four principal conclusions:

(i) We first consider the accretion rate of material contributing to the net growth of galaxies. We find that the presence of feedback strongly suppresses "smooth mode" gas – originating directly from the intergalactic medium, without prior incorporation into a satellite galaxy – at all redshifts. For accretion onto galaxies in $\sim 10^{11.5}\,\mathrm{M_\odot}$ haloes, the rate of smooth accretion is reduced by a factor of ~ 10 by $z = 1$, increasingly so towards $z = 0$. Furthermore, we find that this suppression is independent of the temperature history of newly acquired gas, implying that star formation driven galactic winds have marginal impact on the thermal evolution of smoothly accreting material, and that the presence of winds does not preferentially prevent material as a function of its past virial heating, or lack thereof. In addition to suppressing the net rates, feedback also reduces the raw inflow rates of smooth accretion by a factor of ~ 2, regardless of redshift.

(ii) We examine the spatial distribution, temperature, and dynamics of gas in haloes sufficiently massive to exhibit both inflowing streams of gas at the virial radius and strong feedback driven outflows arising from the central galaxy. Feedback populates the inner halo ($r/r_{\mathrm{vir}} < 0.5$) with a large mass of cold gas with high covering fraction, substantially altering the temperature and velocity structure of halo gas at these small radii. At the virial radius, however, gas inflow is largely unaffected by the introduction of our fiducial feedback model – for example, we find no notable difference in the temperature distribution of inflowing material, nor the inwards radial mass flux, across r_{vir}. The spherical covering fraction of inflowing gas at $0.25\,r_{\mathrm{vir}}$ decreases substantially, at $z = 2$ from more than 80% to less than 50%, while the rates of both inflow and outflow increase, indicative of recycling across this boundary.

(iii) Comparing the relative contribution of different accretion modes – smooth, clumpy (merger), stripped and recycled – we find that the fraction of the total net accretion contributed by smooth accretion is lower in the simulation with feedback, by roughly a factor of two across all redshifts, and particularly so for $T_{\mathrm{max}}\,/\,T_{\mathrm{vir,acc}} < 1$ material at $z < 1$, which is suppressed in the feedback run to a negligible level. Gas which has been recycled through a wind phase prior to its incorporation into a central galaxy makes up a large fraction of total accretion. For gas entering the galaxy for the first time, this fraction is $> 50\%$ at $z < 1$, and between 10% - 50% at $z > 2$.

(iv) As a measure of the timescale of accretion, we calculate the time difference between the first (highest redshift) virial radius crossing and the first incorporation into the galaxy for accreting gas. For smooth accretion, the distribution of these "halo transit times" is uni-modal and broad. The mean transit time increases in the presence of feedback by a factor of $\simeq 2$ - 3, but independent of halo mass. Furthermore, the distribution of these times is *also* independent of

halo mass, at least from $10^{10}\,\mathrm{M_\odot}$ to $10^{12}\,\mathrm{M_\odot}$. This holds true in both runs, with and without feedback, indicating that the timescale of accretion through the halo does not exhibit any sharp transition point in halo mass, above and below which the process of gas accretion proceeds in a fundamentally different manner. The full implications for theory concerning the cooling of hot halo gas, such as those commonly used in semi-analytical models of galaxy formation, remain an important and intriguing direction for future work.

REFERENCES

Abadi M. G., Navarro J. F., Steinmetz M., Eke V. R., 2003, ApJ, 591, 499

Agertz O., Kravtsov A. V., 2014, preprint, (arXiv:1404.2613)

Agertz O., Teyssier R., Moore B., 2009, MNRAS, 397, L64

Agertz O., Kravtsov A. V., Leitner S. N., Gnedin N. Y., 2013, ApJ, 770, 25

Aumer M., White S. D. M., Naab T., Scannapieco C., 2013, MNRAS, 434, 3142

Bachmann L. K., Dolag K., Hirschmann M., Almudena Prieto M., Remus R.-S., 2014, preprint, (arXiv:1409.3221)

Barnes J., Hut P., 1986, Nature, 324, 446

Bauer A., Springel V., 2012, MNRAS, p. 3102

Bellovary J., Brooks A., Volonteri M., Governato F., Quinn T., Wadsley J., 2013, ApJ, 779, 136

Birnboim Y., Dekel A., 2003, MNRAS, 345, 349

Booth C. M., Agertz O., Kravtsov A. V., Gnedin N. Y., 2013, ApJL, 777, L16

Bower R. G., Benson A. J., Malbon R., Helly J. C., Frenk C. S., Baugh C. M., Cole S., Lacey C. G., 2006, MNRAS, 370, 645

Brook C. B., Stinson G., Gibson B. K., Shen S., Macciò A. V., Obreja A., Wadsley J., Quinn T., 2014, MNRAS, 443, 3809

Brooks A. M., Governato F., Quinn T., Brook C. B., Wadsley J., 2009, ApJ, 694, 396

Cen R., 2014, ApJL, 789, L21

Ceverino D., Klypin A., Klimek E. S., Trujillo-Gomez S., Churchill C. W., Primack J., Dekel A., 2014, MNRAS, 442, 1545

Costa T., Sijacki D., Haehnelt M. G., 2014, MNRAS, 444, 2355

Croton D. J., et al., 2006, MNRAS, 365, 11

Danovich M., Dekel A., Hahn O., Teyssier R., 2012, MNRAS, 422, 1732

Danovich M., Dekel A., Hahn O., Ceverino D., Primack J., 2014, preprint, (arXiv:1407.7129)

Davé R., Finlator K., Oppenheimer B. D., 2012, MNRAS, 421, 98

Dekel A., Birnboim Y., 2006, MNRAS, 368, 2

Dekel A., et al., 2009, Nature, 457, 451

Dekel A., Zolotov A., Tweed D., Cacciato M., Ceverino D., Primack J. R., 2013, MNRAS, 435, 999

Dolag K., Borgani S., Murante G., Springel V., 2009, MNRAS, 399, 497

Dubois Y., Pichon C., Devriendt J., Silk J., Haehnelt M., Kimm T., Slyz A., 2012a, preprint (astro-ph/1206.5838),

Dubois Y., Pichon C., Haehnelt M., Kimm T., Slyz A., Devriendt J., Pogosyan D., 2012b, MNRAS, 423, 3616

Dubois Y., et al., 2014, MNRAS, 444, 1453

Faucher-Giguère C.-A., Lidz A., Zaldarriaga M., Hernquist L., 2009, ApJ, 703, 1416

Faucher-Giguère C.-A., Kereš D., Ma C.-P., 2011, MNRAS, 417, 2982

Faucher-Giguere C.-A., Hopkins P. F., Keres D., Muratov A. L., Quataert E., Murray N., 2014, preprint, (arXiv:1409.1919)

Feng Y., Di Matteo T., Croft R., Khandai N., 2014, MNRAS, 440, 1865

Gabor J. M., Bournaud F., 2014, MNRAS, 437, L56

Genel S., Genzel R., Bouché N., Naab T., Sternberg A., 2009, ApJ, 701, 2002

Genel S., Dekel A., Cacciato M., 2012, MNRAS, 425, 788

Genel S., Vogelsberger M., Nelson D., Sijacki D., Springel V., Hernquist L., 2013, MNRAS, 435, 1426

Genel S., et al., 2014, MNRAS, 445, 175

Górski K. M., Hivon E., Banday A. J., Wandelt B. D., Hansen F. K., Reinecke M., Bartelmann M., 2005, ApJ, 622, 759

Hanasz M., Lesch H., Naab T., Gawryszczak A., Kowalik K., Wóltański D., 2013, ApJL, 777, L38

Henriques B., White S., Thomas P., Angulo R., Guo Q., Lemson G., Springel V., Overzier R., 2014, preprint, (arXiv:1410.0365)

Hopkins P. F., Kereš D., Oñorbe J., Faucher-Giguère C.-A., Quataert E., Murray N., Bullock J. S., 2014, MNRAS, 445, 581

Karakas A. I., 2010, MNRAS, 403, 1413

Katz N., Weinberg D. H., Hernquist L., 1996, ApJS, 105, 19

Katz N., Keres D., Dave R., Weinberg D. H., 2003, in Rosenberg J. L., Putman M. E., eds, Astrophysics and Space Science Library Vol. 281, The IGM/Galaxy Connection. The Distribution of Baryons at z=0. p. 185 (arXiv:astro-ph/0209279)

Kereš D., Katz N., Weinberg D. H., Davé R., 2005, MNRAS, 363, 2

Kereš D., Katz N., Fardal M., Davé R., Weinberg D. H., 2009, MNRAS, 395, 160

Kereš D., Vogelsberger M., Sijacki D., Springel V., Hernquist L., 2012, MNRAS, 425, 2027

Khandai N., Di Matteo T., Croft R., Wilkins S. M., Feng Y., Tucker E., DeGraf C., Liu M.-S., 2014, preprint, (arXiv:1402.0888)

Li Y., Bryan G. L., 2014, ApJ, 789, 54

Lu Y., Kereš D., Katz N., Mo H. J., Fardal M., Weinberg M. D., 2011, MNRAS, 416, 660

Monaco P., Benson A. J., De Lucia G., Fontanot F., Borgani S., Boylan-Kolchin M., 2014, MNRAS, 441, 2058

Murante G., Calabrese M., De Lucia G., Monaco P., Borgani S., Dolag K., 2012, ApJL, 749, L34

Nelson D., Vogelsberger M., Genel S., Sijacki D., Kereš D., Springel V., Hernquist L., 2013, MNRAS, 429, 3353

Ocvirk P., Pichon C., Teyssier R., 2008, MNRAS, 390, 1326

Oppenheimer B. D., Davé R., Kereš D., Fardal M., Katz N., Kollmeier J. A., Weinberg D. H., 2010, MNRAS, 406, 2325

Portinari L., Chiosi C., Bressan A., 1998, A & A, 334, 505

Rahmati A., Pawlik A. H., Raičevic M., Schaye J., 2013, MNRAS, 430, 2427

Rees M. J., Ostriker J. P., 1977, MNRAS, 179, 541

Salem M., Bryan G. L., 2014, MNRAS, 437, 3312

Sales L. V., Navarro J. F., Theuns T., Schaye J., White S. D. M., Frenk C. S., Crain R. A., Dalla Vecchia C., 2012, MNRAS, 423, 1544

Sánchez Almeida J., Elmegreen B. G., Muñoz-Tuñón C., Elmegreen D. M., 2014, A&ARv, 22, 71

Sarkar K. C., Nath B. B., Sharma P., Shchekinov Y., 2014, preprint, (arXiv:1409.4874)

Schaye J., et al., 2014, preprint, (arXiv:1407.7040)

Sijacki D., Springel V., Di Matteo T., Hernquist L., 2007, MNRAS, 380, 877

Sijacki D., Vogelsberger M., Kereš D., Springel V., Hernquist L., 2012, MNRAS, 424, 2999

Silk J., 1977, ApJ, 211, 638

Springel V., 2010, MNRAS, 401, 791

Springel V., Hernquist L., 2003, MNRAS, 339, 289

Springel V., White S. D. M., Tormen G., Kauffmann G., 2001, MNRAS, 328, 726

Springel V., Di Matteo T., Hernquist L., 2005, MNRAS, 361, 776

Stewart K. R., Kaufmann T., Bullock J. S., Barton E. J., Maller A. H., Diemand J., Wadsley J., 2011, ApJ, 738, 39

Stewart K. R., Brooks A. M., Bullock J. S., Maller A. H., Diemand J., Wadsley J., Moustakas L. A., 2013, ApJ, 769, 74

Stinson G. S., Brook C., Macciò A. V., Wadsley J., Quinn T. R., Couchman H. M. P., 2013, MNRAS, 428, 129

Sutherland R. S., Dopita M. A., 1993, ApJS, 88, 253

Thielemann F.-K., Nomoto K., Yokoi K., 1986, A & A, 158, 17

Torrey P., Vogelsberger M., Sijacki D., Springel V., Hernquist L., 2012, MNRAS, 427, 2224

Torrey P., Vogelsberger M., Genel S., Sijacki D., Springel V., Hernquist L., 2014, MNRAS, 438, 1985

Übler H., Naab T., Oser L., Aumer M., Sales L. V., White S. D. M., 2014, MNRAS, 443, 2092

Viola M., Monaco P., Borgani S., Murante G., Tornatore L., 2008, MNRAS, 383, 777

Vogelsberger M., Sijacki D., Kereš D., Springel V., Hernquist L., 2012, MNRAS, 425, 3024

Vogelsberger M., Genel S., Sijacki D., Torrey P., Springel V., Hernquist L., 2013, MNRAS, 436, 3031

Vogelsberger M., et al., 2014a, MNRAS, 444, 1518

Vogelsberger M., et al., 2014b, Nature, 509, 177

White S. D. M., Frenk C. S., 1991, ApJ, 379, 52

White S. D. M., Rees M. J., 1978, MNRAS, 183, 341

Wiersma R. P. C., Schaye J., Smith B. D., 2009, MNRAS, 393, 99

Woods R. M., Wadsley J., Couchman H. M. P., Stinson G., Shen S., 2014, MNRAS, 442, 732

Wurster J., Thacker R. J., 2013, MNRAS, 431, 2513

Yoshida N., Stoehr F., Springel V., White S. D. M., 2002, MNRAS, 335, 762

Zhu Q., Hernquist L., Li Y., 2014, preprint, (arXiv:1410.4222)

van Leer B., 1977, Journal of Computational Physics, 23, 276

van de Voort F., Schaye J., Booth C. M., Haas M. R., Dalla Vecchia C., 2011a, MNRAS, 414, 2458

van de Voort F., Schaye J., Booth C. M., Dalla Vecchia C., 2011b, MNRAS, 415, 2782